

Goal-Reaching Trajectory Design Near Danger with Piecewise Affine Reach-avoid Computation

Long Kiu Chung*, Wonsuhk Jung*, Chuizheng Kong, and Shreyas Kousik

Abstract—Autonomous mobile robots must maintain safety, but should not sacrifice performance, leading to the classical *reach-avoid* problem. This paper seeks to compute trajectory plans for which a robot is guaranteed to *reach* a goal and to *avoid* obstacles in the specific *near danger* case that the obstacles and goal are near each other. The proposed method builds off of a common approach of using a simplified planning model to generate plans, which are then tracked using a high-fidelity tracking model and controller. Existing safe planning approaches use reachability analysis to overapproximate the error between these models, but this introduces additional numerical approximation error and thereby conservativeness that prevents goal reaching. The present work instead proposes a Piecewise Affine Reach-avoid Computation (PARC) method to tightly approximate the reachable set of the planning model. With PARC, the main source of conservativeness is the model mismatch, which can be mitigated by careful controller and planning model design. The utility of this method is demonstrated through extensive numerical experiments in which PARC outperforms state-of-the-art reach avoid methods in near-danger goal reaching. Furthermore, in a simulated demonstration, PARC enables generation of provably-safe extreme vehicle dynamics drift parking maneuvers.

I. INTRODUCTION

The increasing deployment of autonomous robots in daily tasks necessitates addressing complex operational challenges. Many of these tasks can be conceptualized as *reach-avoid* problems, wherein a robot must steer its states into a set of goal states without violating safety-critical constraints [1]. Achieving both *liveness* – the assurance of goal fulfillment [2] – and adherence to safety constraints is pivotal in these scenarios. In this paper, we are particularly interested in goal reaching *near danger*, meaning that an obstacle is near enough to a desired goal location to prevent typical robust planning or control approaches from reaching the goal. This often occurs when a goal and obstacles are closer to each other than one width of a robot’s body, such as for a quadrotor drone flying through a narrow gap or an autonomous car parallel parking.

The reach-avoid problem is typically solved with one of two approaches, both based on reachability analysis or computing reachable sets of a system’s trajectories. Note that an extended literature review is presented in Appendix A. The first approach is *control intervention*, wherein a motion planner proposes actions, while a safety filter [3],

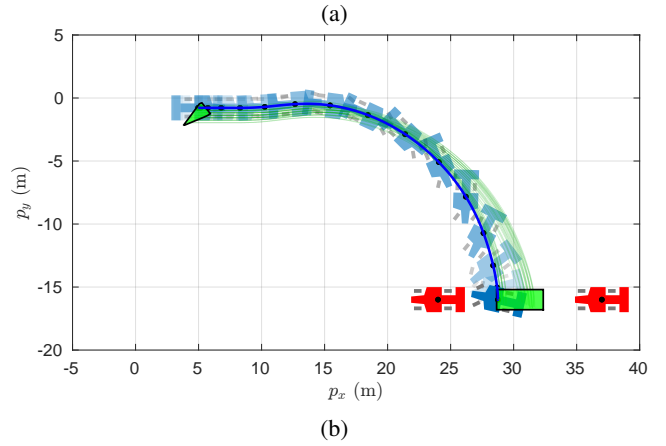
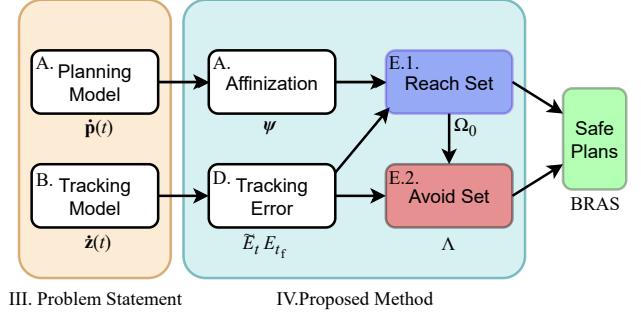


Fig. 1: Our overall goal is to find safe goal-reaching motion plans near danger. In (a), we show the components of our proposed Piecewise Affine Reach-avoid Computation (PARC) method, with the paper section number on the top left, and the corresponding symbol on the bottom. This method enables a new state-of-the-art for safe reach-avoid problems, as evidenced by (b), which shows examples of extreme vehicle maneuvers. These planned drift parking trajectories are sampled from the Backward Reach-Avoid Set (BRAS, green triangle on the top left) using PARC. Our vehicle is in a blue time lapse. The two red cars are obstacles. The goal set for the center of mass is the green rectangle. The small size of the BRAS indicates the challenge of finding safe trajectories.

[4] prevents the robot from executing actions for which its reachable set would intersect obstacles. This approach often requires compensating for the worst-case behavior of the motion planner [5], [6], which we find leads to conservativeness (i.e., sacrificing liveness) in our experiments (Section V). The second approach is a *planner-tracker* framework, wherein a motion planner proposes plans that are safe by leveraging the knowledge of a low-level controller’s tracking ability. This controller can be synthesized [7], [8] or hand-engineered [9], [10]; the key difference is that the planner need not be treated as adversarial, which reduces conservativeness. However, this approach typically limits the space of possible

* indicates the equal contribution. All authors are with the School of Mechanical Engineering at the Georgia Institute of Technology, Atlanta, GA. (e-mail: {lchung33, wonsuhk.jung, ckong35}@gatech.edu; shreyas.kousik@me.gatech.edu).

Project: <https://saferoboticslab.me.gatech.edu/research/parc/>,

Github: <https://github.com/safe-robotics-lab-gt/PARC>

plans due to the need to compute the robot's tracking ability. Furthermore, one must compensate for *tracking error* between the simplified *planning model* and the high-fidelity *tracking model* (i.e., the robot cannot perfectly track plans).

Both control intervention and planner-tracker approaches suffer from challenges in numerical representation due to the need to *underapproximate* the set of states that reach the target set and *overapproximate* those that avoids obstacles when guaranteeing safety and liveness in implementation. Implementations such as sums-of-squares polynomials [7], [9], [11], grid-based PDE solutions [5], or polytope methods [10], [12] all introduce additional conservativeness purely due to compensating for numerical representation error. This challenge is exacerbated for systems with high-dimensional, nonlinear dynamics or observations; machine learning can address some of these concerns [13]–[17], at the expense of losing guarantees.

In this work, we leverage two key insights to perform the goal-reaching near danger. First, as mentioned before, planner-tracker methods can reduce conservativeness by treating the planner and tracking controller as cooperative, as opposed to adversarial. Second, by representing our motion planner as a *piecewise affine* (PWA) system [18], we can *tightly approximate* its reachable set, with conservativeness mainly due to tracking controller and planning model design. We build off of a long history of discrete-time PWA system analysis in optimal control (e.g., [19]–[21]), which we extend to the continuous-time reach-avoid problem for robot motion planning. We demonstrate that this unlocks a faster and less conservative approach to a variety of reach-avoid problems from the robotics literature, and provides the solution to a reachable set computation for drift parking vehicle dynamics. An overview and example of our approach is shown in Fig. 1.

Contributions:

- 1) We propose an efficient, parallelizable method for Piecewise Affine Reach-avoid Computation (PARC) to underapproximate the Backwards Reach-Avoid Set (BRAS) of a planning model represented as a low-dimensional discrete-time, time-variant PWA system. Our method extends to discrete-time, time-variant affine systems as a particular case.
- 2) We propose a scheme to incorporate tracking error into PARC to underapproximate the *reach set* and overapproximate the *avoid set* for a trajectory planning model. This allows us to represent the BRAS that compactly represents all trajectory plans that reach the goal and avoid obstacles when tracked by the robot, represented by a high-fidelity dynamical model.
- 3) We stress-test PARC on examples drawn from the safe control and planning literature: a 4-D TurtleBot, a 10-D near-hover quadrotor, and a 13-D quadrotor. We show that PARC outperforms state-of-the-art methods such as FaSTrack [5], Neural CLBF [15], and RTD [9], [10]. We also demonstrate PARC on a simulated 6-D vehicle model to plan safe, extreme drift parallel parking maneuvers.

Paper Organization: Next, we introduce mathematical

objects used throughout our formulation (Section II). We then present our problem formulation (Section III) and proposed approach (Section IV). We assess PARC with numerical experiments (Section V), then demonstrate a drift parking extreme vehicle dynamics example in simulation, extending beyond the state of the art in reachability-based safe motion-planning and control methods (Section VI). We discuss takeaways and limitations in Section VII. Note, we have extensive appendices, and call out **key results** in the text.

II. PRELIMINARIES

We now introduce our notation conventions and define H-polytopes and PWA functions, which we use to represent sets and dynamics of planning model throughout the paper. We then present a one-step Backward Reachable Set (BRS) computation that is the core of our proposed PARC method.

A. Notation

The real numbers are \mathbb{R} and the natural numbers are \mathbb{N} . Scalars are lowercase italic and sets are in uppercase italic (e.g., $a \in A \subset \mathbb{R}^n$). Vectors are lowercase bold, and matrices are uppercase bold (e.g., $\mathbf{y} = \mathbf{A}\mathbf{x}$). An $n \times m$ matrix of zeros is $\mathbf{0}_{n \times m}$, and an $n \times n$ identity matrix is \mathbf{I}_n . The p^{th} to q^{th} dimensions of vector \mathbf{x} and the submatrix of \mathbf{A} defined by row dimensions $p_1:q_1$ and column dimensions $p_2:q_2$ are denoted as $(\mathbf{x})_{p:q}$ and $(\mathbf{A})_{p_1:q_1, p_2:q_2}$, respectively.

B. H-Polytopes

In this work, we represent all sets as H-polytopes or unions of H-polytopes, which have extensive algorithm and toolbox support [22], [23]. An n -dimensional H-polytope $\mathcal{P}(\mathbf{A}, \mathbf{b}) \subset \mathbb{R}^n$ is a convex set parameterized by n_h linear constraints $\mathbf{A} \in \mathbb{R}^{n_h \times n}$ and $\mathbf{b} \in \mathbb{R}^{n_h}$:

$$\mathcal{P}(\mathbf{A}, \mathbf{b}) = \{\mathbf{x} \mid \mathbf{A}\mathbf{x} \leq \mathbf{b}\}. \quad (1)$$

Unless otherwise stated, we assume all H-polytopes are compact.

Consider a pair of H-polytopes $P_1 = \mathcal{P}(\mathbf{A}_1, \mathbf{b}_1)$, $P_2 = \mathcal{P}(\mathbf{A}_2, \mathbf{b}_2)$. We make use of intersections $P_1 \cap P_2$, Minkowski sums $(P_1 \oplus P_2 = \{\mathbf{x} + \mathbf{y} \mid \mathbf{x} \in P_1, \mathbf{y} \in P_2\})$, Pontryagin differences $(P_1 \ominus P_2 = \{\mathbf{x} \in P_1 \mid \mathbf{x} + \mathbf{y} \in P_2 \forall \mathbf{y} \in P_2\})$, set differences $P_1 \setminus P_2$, Cartesian products $P_1 \times P_2$, and convex hulls $\text{conv}(P_1, P_2)$. We also project an n -dimensional polytope P into dimensions $p:q$ as $\text{proj}_{p:q}(P)$. These operations are detailed in Appendix B.

C. PWA Systems

We consider discrete-time, time-variant PWA functions to enable our reach-avoid analysis. We denote a PWA function as $\psi: X_0 \rightarrow X_{t_f} \subseteq \mathbb{R}^n$ with output $\mathbf{x}(t_f) = \psi(\mathbf{x}(0))$ given an input $\mathbf{x}(0) = \mathbf{x}_0 \in X_0 \subset \mathbb{R}^n$. The system has state $\mathbf{x}(t) \in X_t \subset \mathbb{R}^n$ at time $t = 0, \Delta t, \dots, t_f - \Delta t$, which is the solution of difference equation of dynamics:

$$\mathbf{x}(t + \Delta t) = \mathbf{C}_{\ell, t} \mathbf{x}(t) + \mathbf{d}_{\ell, t}, \quad (2)$$

where $\mathbf{C}_{\ell,t} \in \mathbb{R}^{n \times n}$ and $\mathbf{d}_{\ell,t} \in \mathbb{R}^n$ define the dynamics of the ℓ^{th} PWA region. The index ℓ is given by

$$\ell = \min\{i \mid \mathbf{x}(t) \in \mathcal{P}(\mathbf{A}_{i,t}, \mathbf{b}_{i,t}), i = 1, \dots, n_{\text{PWA},t}\}, \quad (3)$$

where $\mathcal{P}(\mathbf{A}_{i,t}, \mathbf{b}_{i,t})$ is the i^{th} of the $n_{\text{PWA},t}$ PWA regions at time t . We say that $\mathbf{x}(t)$ has the *mode* $s_t = \ell$ at time t .

In addition, if the mode of $\mathbf{x}(0), \mathbf{x}(\Delta t), \dots, \mathbf{x}(t_f - \Delta t)$ is $s_0, s_{\Delta t}, \dots, s_{t_f - \Delta t}$ for some input $\mathbf{x}(0) \in X_0$, we denote the *mode sequence* for $\mathbf{x}(0)$ as:

$$S = (s_0, s_{\Delta t}, \dots, s_{t_f - \Delta t}). \quad (4)$$

For all $\mathbf{x}(0)$ that share the same mode sequence, the dynamics reduce from time-variant PWA to time-variant affine up to time t_f . This is the core idea that enables the efficient underapproximating BRS computation of PARC. Note, taking advantage of fixed mode sequences is well-established in robotics and controls (e.g., [19], [20], [24], [25]), but we believe we are the first to show its utility in safe reach-avoid computation of robot planning models.

We require that the interior of each PWA region does not intersect with other regions, such that any two regions are either disjoint or intersect only at their boundaries:

$$\{\mathbf{x} \mid \mathbf{A}_i(t)\mathbf{x} < \mathbf{b}_i(t)\} \cap \mathcal{P}(\mathbf{A}_j(t), \mathbf{b}_j(t)) = \emptyset, \quad (5)$$

for all $t = 0, \Delta t, \dots, t_f - \Delta t$ and $i, j \in \{1, \dots, n_{\text{PWA},t}\}$, $i \neq j$. Thus, the min in (3) dictates the dynamics' behavior at the intersecting subsets of boundaries.

Note that, for $t = 0, \Delta t, \dots, t_f - \Delta t$, we define:

$$X_t = \bigcup_{i=1}^{n_{\text{PWA},t}} \mathcal{P}(\mathbf{A}_{i,t}, \mathbf{b}_{i,t}), \quad (6)$$

such that the input to ψ is restricted to $\{\mathbf{x}_0 \mid \mathbf{x}_t \in X_t, t = 0, \Delta t, \dots, t_f - \Delta t\}$. Thus, a PWA function ψ can be fully defined and parameterized by some given $\mathbf{C}_{i,t}$, $\mathbf{d}_{i,t}$, $\mathbf{A}_{i,t}$, and $\mathbf{b}_{i,t}$ for each $i = 1, \dots, n_{\text{PWA},t}$ and $t = 0, \Delta t, \dots, t_f - \Delta t$.

When $n_{\text{PWA},t} = 1$ for all $t = 0, \Delta t, \dots, t_f - \Delta t$, one obtains a discrete-time, time-variant affine system as a particular case of this problem formulation.

Finally, to ensure safety for realistic systems, we must extend our system definition from discrete to continuous time. We do so with linear interpolation: at each $t = 0, \Delta t, \dots, t_f - \Delta t$, $\mathbf{x}(t')$ for $t < t' < t + \Delta t$ is defined by

$$\mathbf{x}(t') = \mathbf{x}(t) + (\mathbf{x}(t + \Delta t) - \mathbf{x}(t)) \left(\frac{t' - t}{\Delta t} \right). \quad (7)$$

D. One Step BRS via Inverse Affine Map

Finally, we take advantage of the H-polytope analytic solution for inverse affine maps to enable BRS computation using the following well-known lemma (c.f., [19], [22], [26]).

Lemma 1. Consider an affine system $\mathbf{x}(t + \Delta t) = \mathbf{C}\mathbf{x}(t) + \mathbf{d}$. Define the one-step BRS as the map $\mathcal{B}(\mathcal{P}(\mathbf{A}, \mathbf{b}), \mathbf{C}, \mathbf{d}) = \{\mathbf{x} \mid \mathbf{A}\mathbf{x}_{\text{next}} \leq \mathbf{b}, \mathbf{x}_{\text{next}} = \mathbf{C}\mathbf{x} + \mathbf{d}\}$. This one-step BRS is in fact an H-polytope:

$$\mathcal{B}(\mathcal{P}(\mathbf{A}, \mathbf{b}), \mathbf{C}, \mathbf{d}) = \mathcal{P}(\mathbf{AC}, \mathbf{b} - \mathbf{Ad}). \quad (8)$$

Proof.

$$\mathcal{B}(\mathcal{P}(\mathbf{A}, \mathbf{b}), \mathbf{C}, \mathbf{d}) = \{\mathbf{x} \mid \mathbf{A}(\mathbf{C}\mathbf{x} + \mathbf{d}) \leq \mathbf{b}\}, \quad (9)$$

$$= \mathcal{P}(\mathbf{AC}, \mathbf{b} - \mathbf{Ad}). \quad (10)$$

□

We take advantage of the fact that repeated applications of Lemma 1 to an H-polytope still produce an H-polytope. Notice that (8) does not require invertibility of \mathbf{C} , conferring an advantage over other set polytope representations such as constrained zonotopes [27]. This makes H-polytopes an excellent choice for representing the BRS.

III. PROBLEM STATEMENT

Our overall goal is to design a reach-avoid trajectory using a simple *planning model*, which enables computational efficiency while also accounting for the tracking error when the plan is tracked by a robot, represented by a *tracking model*. We now describe each of these models and the problem we seek to solve.

A. Planning Model

A planning model provides a low-fidelity but fast-to-compute model of the robot's dynamics. In this work, we use parameterized reference trajectories, which can allow quick computation and strong safety guarantees [9], [10], [28].

Before defining the model, we define a workspace state $\mathbf{w} \in W \subset \mathbb{R}^{n_w}$ (i.e., \mathbb{R}^2 or \mathbb{R}^3) that represents the position of the robot. The planning state which we denote as $\mathbf{p} \in P \subset \mathbb{R}^{n_p}$ is chosen to include the workspace state, such that $\mathbf{p} = [\mathbf{w}^\top, \mathbf{p}_{\text{other}}^\top]^\top$ where $\mathbf{p}_{\text{other}} \in P_{\text{other}} \subset \mathbb{R}^{n_{\text{pother}}}$ represents states such as heading, velocity, etc.

We then define the planning model as

$$\dot{\mathbf{p}}(t) = \mathbf{f}_{\text{plan}}(t, \mathbf{p}(t), \mathbf{k}), \quad \mathbf{p}(0) = \mathbf{p}_0 \quad (11)$$

where $\mathbf{p}_0 \in P \subset \mathbb{R}^{n_p}$ defines the *initial planning state*, $\mathbf{k} \in K \subset \mathbb{R}^{n_k}$ represents a *trajectory parameter*, and $t \in [0, t_f]$ is the time horizon. A solution $\mathbf{p} : [0, t_f] \rightarrow P$ is referred to as a *plan*, or equivalently, *reference trajectory*. For a given initial planning state and trajectory parameter, the plan at time t is $\mathbf{p}(t; \mathbf{p}_0, \mathbf{k})$. We restrict the class of planning models to enable computing reachable sets for parameterized planning models:

Assumption 2 (Extended Translation Invariance (ETI) in Workspace). Changing the workspace state either does not affect the planning dynamics \mathbf{f}_{plan} in the workspace or else the dynamics are constant:

$$\left\| \frac{\partial \mathbf{f}_{\text{w}}}{\partial \mathbf{w}} \mathbf{f}_{\text{w}} \right\|_2 = 0 \quad \text{and} \quad \left\| \frac{\partial \mathbf{f}_{\text{w}}}{\partial \mathbf{w}} \frac{\partial \mathbf{f}_{\text{w}}}{\partial \mathbf{p}} \right\|_{\text{F}} = 0, \quad (12)$$

where $\mathbf{f}_{\text{w}} = (\mathbf{f}_{\text{plan}})_{1:n_w}$ and $\|\cdot\|_{\text{F}}$ indicates the Frobenius norm.

This is not overly restrictive; a variety of ETI planning models are shown in Section V. The need for the dynamics to be constant in some states is because we treat \mathbf{k} as states with 0 dynamics to formulate our reachability method.

B. Tracking Model

The tracking model is a high-fidelity model of robot dynamics, denoted

$$\dot{\mathbf{z}}(t) = \mathbf{f}_{\text{track}}(\mathbf{z}(t), \mathbf{u}_{\text{fb}}(t)), \quad \mathbf{z}(0) = \mathbf{z}_0, \quad (13)$$

where $\mathbf{z}_0 \in Z \subset \mathbb{R}^{n_z}$ is the initial state. The tracking state \mathbf{z} includes the planning state \mathbf{p} , i.e., $\mathbf{z} = [\mathbf{p}^\top, \mathbf{z}_{\text{other}}^\top]^\top$. Given a plan \mathbf{p} parameterized by \mathbf{k} , we use a feedback tracking controller $\mathbf{u}_{\text{fb}}(t, \mathbf{z}(t); \mathbf{k}) \in U$ (e.g., PID or MPC) to control the tracking model. We assume Z and U are compact and the dynamics are Lipschitz such that trajectories exist [29]. For a particular \mathbf{z}_0 , we denote the resulting, unique *realized trajectory* (i.e., solution to (13)) as $\mathbf{z}(t; \mathbf{z}_0, \mathbf{k})$ at time t .

Remark 3. Designing the feedback controller \mathbf{u}_{fb} is not the focus of this work. Conveniently, specifying a parameterized (i.e., restricted) space of plans \mathbf{p} simplifies controller design. Our overall goal is to compensate for the fact that the controller is imperfect.

C. Reach-Avoid Problem

We now define our reach-avoid problem: find all plans for which the tracking model safely reaches a goal set at time t_f . We denote the goal $\overline{P_G} \subset W$ and obstacles $\overline{O} \subset W$; the overline indicates these are restricted to the workspace, which we modify later to enable the proposed method.

Note, we only consider static obstacles, because our goal is to plan a robot's motion near danger. The danger resulting from moving or adversarial obstacles depends upon accurately predicting obstacle motion, which introduces an independent variable unrelated to our purpose. We leave extension to dynamic scenes for future work; we anticipate we can adapt reachability-based methods such as [30].

Problem 4 (Backward Reach-Avoid Set (BRAS)). *Given the planning model (11), tracking model (13), goal set $\overline{P_G}$, obstacles \overline{O} , and a fixed time t_f , find the set of planning models states and trajectory parameters for which the robot reaches $\overline{P_G}$ exactly at time t_f while avoiding collisions with obstacles \overline{O} :*

$$\begin{aligned} \text{BRAS}(t_f, \overline{P_G}, \overline{O}) = \{(\mathbf{p}_0, \mathbf{k}) \in P \times K \mid \forall \mathbf{z}_0 \text{ s.t.} \\ (\mathbf{z}_0)_{1:n_w} = \mathbf{p}_0, \\ (\mathbf{z}(t_f; \mathbf{z}_0, \mathbf{k}))_{1:n_w} \in \overline{P_G}, \text{ and} \\ (\mathbf{z}(\tau; \mathbf{z}_0, \mathbf{k}))_{1:n_w} \notin \overline{O} \quad \forall \tau \in [0, t_f]\} \end{aligned} \quad (14)$$

Remark 5. A fixed time horizon is reasonable because we seek to compute a trajectory near danger; the robot is already near its goal, but reaching the goal is difficult. The BRAS is a large set far from obstacles that can be used as a target set for other methods to reach safely.

Remark 6. We restrict the goal and obstacles to the workspace only to simplify exposition; we demonstrate more general goals and obstacles, such as in the robot's orientation, in Sections V and VI.

D. Example System: TurtleBot

We use the TurtleBot unicycle model as an illustrative example from the safe planning and control literature [5], [9]. Our planning model is a Dubins car:

$$\dot{\mathbf{p}} = \frac{d}{dt} \begin{bmatrix} p_x \\ p_y \\ \theta \end{bmatrix} = \begin{bmatrix} v_{\text{des}} \cos \theta \\ v_{\text{des}} \sin \theta \\ \omega_{\text{des}} \end{bmatrix}, \quad (15)$$

with workspace (position) states $\mathbf{w} = [p_x, p_y]^\top$, other (heading) state $\mathbf{p}_{\text{other}} = \theta$, and trajectory parameters $\mathbf{k} = [v_{\text{des}}, \omega_{\text{des}}]^\top$. Note that a Dubins car model (15) is ETI in the workspace (Assum. 2) since its dynamics in workspace dimension is translation-invariant (i.e. $\left\| \frac{\partial \mathbf{f}_{\mathbf{w}}}{\partial \mathbf{w}} \right\|_2 = 0$).

We use the following tracking model:

$$\dot{\mathbf{z}} = \frac{d}{dt} \begin{bmatrix} p_x \\ p_y \\ \theta \\ v \\ u_\omega \\ u_v \end{bmatrix} = \begin{bmatrix} v \cos \theta \\ v \sin \theta \\ u_\omega \\ u_v \end{bmatrix}, \quad (16)$$

where $\mathbf{z}_{\text{other}} = [\theta, v]^\top$ are heading and linear velocity, and $\mathbf{u}_{\text{fb}} = [u_\omega, u_v]^\top$ is implemented as an iterative LQR tracking controller [31] that commands angular velocity and linear acceleration.

We define a goal set as a unit box, $\overline{P_G} = \{\mathbf{w} \mid p_x, p_y \in [-1, 1]\}$, and an obstacle near the goal, $\overline{O} = \{\mathbf{w} \mid p_x \in [-2.5, -1.5], p_y \in [-1, 0]\}$ (see Figures 2 and 3).

IV. PROPOSED METHOD

In this section, we detail our approach to solving the BRAS problem. First, we convert the planning model to a PWA system to enable our Piecewise Affine Reach-Avoid Computation (PARC). We then adapt the method in [19] to underapproximate the reach set of the PWA planning model *without* tracking error, to simplify exposition. Next, we propose a novel approach to *overapproximate* the continuous time avoid set of the PWA system without tracking error (**Key result:** Theorem 11). To enable incorporating tracking error between the planned and realized trajectories, we adapt the methods in [9], [10] to estimate time-varying tracking error. Finally, we propose PARC to incorporate tracking error and compute the BRAS (**Key result:** Theorem 17), enabling provably-safe goal-reaching.

A. Reformulation to Enable PARC

1) *Augmented State, Goal, and Obstacles:* Before proceeding, to enable PARC, we define an *augmented planning state* $\mathbf{x}(t) \in X = W \times K \times P_{\text{other}} \subset \mathbb{R}^{n_w + n_k + n_{p_{\text{other}}}}$ at time t as:

$$\mathbf{x}(t) = \begin{bmatrix} \mathbf{w}(t) \\ \mathbf{k} \\ \mathbf{p}_{\text{other}}(t) \end{bmatrix}. \quad (17)$$

We perform this reordering and stacking because, as we see later in Lem. 10, the \mathbf{w} and \mathbf{k} are ETI states, so it indexing them as the first states of \mathbf{x} simplifies avoid set computation.

We similarly augment the goal set \overline{P}_G and the obstacles $\overline{\mathcal{O}} = \bigcup_{i=1}^{n_o} \mathcal{O}_i$, which we assume are union of H-polytopes:

$$\begin{aligned} P_G &= \overline{P}_G \times K \times P_{\text{other}} \\ \mathcal{O}_i &= \overline{\mathcal{O}}_i \times K \times P_{\text{other}}. \end{aligned} \quad (18)$$

2) PWA Planning Model: We approximate the planning model \mathbf{f}_{plan} as a discrete-time, time-variant PWA to enable computation. First, we define linearization points $\mathbf{x}_{i,t}^* \in X_t$, $i = 1, \dots, n_t^*$ for each $t = 0, \Delta t, \dots, t_f - \Delta t$, which can be generated by gridding or uniform sampling. We define the PWA regions as the Voronoi partition of the linearization points [32] (see Appendix C). Each i^{th} region is an H-polytope $\mathcal{P}(\mathbf{A}_{i,t}, \mathbf{b}_{i,t})$. Then, in each region, at each time $t = 0, \Delta t, \dots, t_f - \Delta t$, we define the dynamics $\mathbf{C}_{i,t}$ and $\mathbf{d}_{i,t}$ by Taylor expanding about the linearization points:

$$\mathbf{x}(t + \Delta t) = \mathbf{g}_{\text{plan},t}(t, \mathbf{x}_{i,t}^*) + \frac{\partial \mathbf{g}_{\text{plan},t}(t, \mathbf{x}(t))}{\partial \mathbf{x}(t)} \Big|_{\mathbf{x}=\mathbf{x}_{i,t}^*} (\mathbf{x}(t) - \mathbf{x}_{i,t}^*), \quad (19a)$$

$$\mathbf{g}_{\text{plan},t}(t, \mathbf{x}(t)) = \begin{bmatrix} (\mathbf{p}(t) + \Delta t \mathbf{f}_{\text{plan}}(t, \mathbf{p}(t), \mathbf{k}))_{1:n_w} \\ \mathbf{k} \\ (\mathbf{p}(t) + \Delta t \mathbf{f}_{\text{plan}}(t, \mathbf{p}(t), \mathbf{k}))_{n_w+1:n_p} \end{bmatrix} \quad (19b)$$

$$\mathbf{C}_{i,t} = \frac{\partial \mathbf{g}_{\text{plan},t}(t, \mathbf{x}(t))}{\partial \mathbf{x}(t)} \Big|_{\mathbf{x}=\mathbf{x}_{i,t}^*}, \quad \text{and} \quad (19c)$$

$$\mathbf{d}_{i,t} = \mathbf{g}_{\text{plan},t}(t, \mathbf{x}_{i,t}^*) - \frac{\partial \mathbf{g}_{\text{plan},t}(t, \mathbf{x}(t))}{\partial \mathbf{x}(t)} \Big|_{\mathbf{x}=\mathbf{x}_{i,t}^*} \mathbf{x}_{i,t}^*. \quad (19d)$$

Depending on the planning model, there may be some PWA regions with identical dynamics. If the union of the regions is convex, we combine them into a single PWA region (note, the linearization points are discarded).

B. Backward Reach Set without Tracking Error

Without accounting for tracking error, the reach set of a planning model is the set of initial conditions \mathbf{x}_0 of trajectories that are *guaranteed* to reach the goal region P_G at time t_f . Instead of naively computing the *full* reach set, which scales exponentially in memory, computation time, and a number of set representations with the number of timesteps, PARC is *planning aware*: given an *expert plan*, we compute only a local, underapproximated BRS efficiently for the neighborhood that shares the same mode sequence as the *expert plan*. Fixing the mode sequence reduces the PWA system to a time-variant affine system, so the BRS is a *single* H-polytope using the inverse affine map of the goal (see (8)), with computation time scaling linearly with the number of timesteps and quadratically with dimensions from matrix multiplication.

Assumption 7 (Expert Plan w/o Tracking Error). *We have access to at least one goal-reaching initial condition \mathbf{x}_0 for which the PWA system reaches the goal without necessarily avoiding obstacles:*

$$\psi(\mathbf{x}_0) \in P_G. \quad (20)$$

Obtaining expert plans is system-dependent, but is not difficult, because we do not require the expert plan to avoid obstacles. Thus, one option is to solve a two-point boundary value nonlinear MPC problem, for which solution guarantees exist [33]. In practice, it is often sufficient to uniformly sample trajectory parameters \mathbf{k} and roll out the PWA planning model, since the robot starts out near the goal. This assumption is even easier to fulfill if the planning model is time-variant affine (which we use for a general 3D quadrotor and drift vehicle planning in Section V, VI) since plans have only one mode.

If Assumption 7 is satisfied, we can obtain \mathbf{x}_0 's mode sequence $S = (s_0, \dots, s_{t_f - \Delta t})$ using (3). That is,

$$s_t = \min\{i \mid \mathbf{x}(t) \in \mathcal{P}(\mathbf{A}_{i,t}, \mathbf{b}_{i,t}), i = 1, \dots, n_{\text{PWA},t}\}, \quad (21)$$

for all $t = 0, \Delta t, \dots, t_f - \Delta t$. Then, we can compute the exact t_f -time BRS using the method in [19]:

Proposition 8 (Reach Set w/o Tracking Error). *Consider a mode sequence $S = (s_0, \dots, s_{t_f - \Delta t})$. Then the exact t_f -time BRS $\overline{\Omega}_0$ of the goal for the affine dynamics associated with S is*

$$\begin{aligned} \overline{\Omega}_{t_f} &= P_G, \\ \overline{\Omega}_t &= \mathcal{B}(\overline{\Omega}_{t+\Delta t}, \mathbf{C}_{s_t,t}, \mathbf{d}_{s_t,t}) \end{aligned} \quad (22)$$

for all $t = 0, \Delta t, \dots, t_f - \Delta t$.

Proof. This follows directly from Lemma 1. \square

This means the reference trajectories generated from any augmented planning state within $\overline{\Omega}_0$ are guaranteed to reach P_G at time t_f with mode sequence S . This process, along with an expert plan, is illustrated in Fig. 2.

C. PARC: Avoid Set without Tracking Error

Without accounting for tracking error, the avoid set is the set of pairs of initial planning model state and trajectory parameter such that any plans generated from *outside* the avoid set are guaranteed to not collide with the obstacles at all *continuous* time before t_f . Recall that, per (7), we model the continuous-time behavior as straight line segments between the discrete states of the PWA system.

Intuitively, the avoid set identifies all trajectories where the straight lines connecting the PWA planning model's discrete states collide with any obstacles:

Proposition 9 (Unsafe Plans w/o Tracking Error). *Consider the obstacle \mathcal{O}_i , some time $t \in \{0, \Delta t, \dots, t_f - \Delta t\}$, and the mode sequence $S = (s_0, \dots, s_t, s_{t+\Delta t}, \dots, s_{t_f - \Delta t})$. Suppose we compute the $(t_f - t)$ -time BRS $\overline{\Omega}_t$ and the $(t_f - t - \Delta t)$ -time BRS $\overline{\Omega}_{t+\Delta t}$ as in (22). If any trajectories between $\overline{\Omega}_t$ and $\overline{\Omega}_{t+\Delta t}$ collide with \mathcal{O}_i , that is, if $\exists \mathbf{x}(t) \in \overline{\Omega}_t, \mathbf{x}(t + \Delta t) = \mathbf{C}_{s_t,t} \mathbf{x}(t) + \mathbf{d}_{s_t,t} \in \overline{\Omega}_{t+\Delta t}$ such that*

$$\mathcal{O}_i \cap \{\mathbf{x}(t) + \gamma(\mathbf{x}(t + \Delta t) - \mathbf{x}(t)) \mid 0 \leq \gamma \leq 1\} \neq \emptyset, \quad (23)$$

then

$$\mathcal{O}_i \cap \text{conv}(\overline{\Omega}_t, \overline{\Omega}_{t+\Delta t}) \neq \emptyset. \quad (24)$$

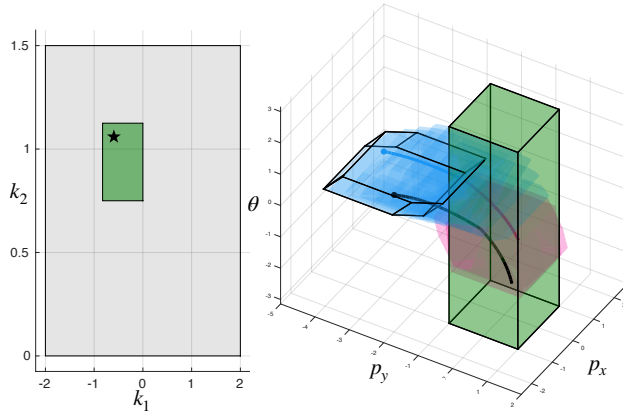


Fig. 2: (Right) Visualization of the reach set computation in Section IV-B for the TurtleBot example (Section III-D), projected onto the planning state space P , when $\mathbf{p}_0 = [-4, 0, \pi/5]^\top$, $t_f = 4(s)$. The goal set is the green polytope extended to all $\theta \in [-\pi, \pi]$. An expert plan, computed by solving a two-point boundary value problem, passes through two modes (blue and magenta line). We compute the corresponding t_f -time BRS $\bar{\Omega}_0$ (blue polytope with solid outline). Intermediate BRSs $\bar{\Omega}_t$ are the polytopes without outlines, colored by mode. (Left) Illustration of the trajectory parameter space; the grey region represents K , the green region represents the projection of $\bar{\Omega}_0$ on K . After reach-set computation, the state $\mathbf{x}_{\text{sample}} = [\mathbf{p}_{\text{sample}}^\top, \mathbf{k}_{\text{sample}}^\top]^\top$ is sampled from $\bar{\Omega}_0$: black dot (right) denotes the $\mathbf{p}_{\text{sample}}$ and black star (left) denotes the $\mathbf{k}_{\text{sample}}$. The resulting trajectory is denoted as the black line which reaches the goal.

Proof. By the definition of convex-hull, we have

$$\text{conv}(\bar{\Omega}_t, \bar{\Omega}_{t+\Delta t}) = \{\mathbf{x}(t) + \gamma(\mathbf{x}(t+\Delta t) - \mathbf{x}(t)) \mid 0 \leq \gamma \leq 1, \mathbf{x}(t), \mathbf{x}(t+\Delta t) \in \bar{\Omega}_t \cup \bar{\Omega}_{t+\Delta t}\}, \quad (25a)$$

$$\supset \{\mathbf{x}(t) + \gamma(\mathbf{x}(t+\Delta t) - \mathbf{x}(t)) \mid 0 \leq \gamma \leq 1, \mathbf{x}(t) \in \bar{\Omega}_t, \mathbf{x}(t+\Delta t) \in \bar{\Omega}_{t+\Delta t}\}. \quad (25b)$$

Thus (23) necessarily implies (24). \square

Next, before we can overapproximate the avoid set between two-time steps, we must adapt our notion of extended translation invariance to the PWA planning model:

Lemma 10 (PWA ETI). *Suppose \mathbf{f}_{plan} is an ETI system in the workspace as in Assum. 2. Also suppose we convert it to a PWA system as in Section IV-A.2 and (19). Then in mode i at time t , each state \mathbf{x} of the PWA system obeys*

$$\|\hat{\mathbf{C}}_{i,t}^W (\hat{\mathbf{C}}_{i,t} \mathbf{x} + \mathbf{d}_{i,t})_{1:n_w}\|_2 = 0 \quad \forall \mathbf{x} \in \mathcal{P}(\mathbf{A}_{i,t}, \mathbf{b}_{i,t}) \quad (26)$$

where $\hat{\mathbf{C}}_{i,t} = \mathbf{C}_{i,t} - \mathbf{I}_{n_x}$ and $\hat{\mathbf{C}}_{i,t}^W$ denotes the $n_w \times n_w$ upper-left submatrix of $\hat{\mathbf{C}}_{i,t}$, namely $\hat{\mathbf{C}}_{i,t}^W \triangleq (\hat{\mathbf{C}}_{i,t})_{1:n_w, 1:n_w}$

Proof. This follows directly from Assum. 2 and (19). \square

The definition of PWA-ETI (26) in other subspace is similarly defined by substituting W to the subspace of interest. Note that \mathbf{f}_{plan} is an ETI system in $W \times K$ since the trajectory parameter $\mathbf{k} \in K$ is constant.

Now, for avoid-set computation, it is helpful to relabel the ETI states of $\mathbf{x}(t)$, identified per Lemma 10:

$$\mathbf{x}(t) = \begin{bmatrix} \mathbf{x}_{\text{ETI}}(t) \\ \mathbf{x}_{\text{other}}(t) \end{bmatrix}, \quad (27)$$

where $\mathbf{x}_{\text{ETI}}(t) \in X_{\text{ETI}} \subset \mathbb{R}^{n_{\text{ETI}}}$ are the first n_{ETI} states in $\mathbf{x}(t)$ that are ETI-states, and $\mathbf{x}_{\text{other}}(t) \in X_{\text{other}} \subset \mathbb{R}^{n_{\text{other}}}$ are the remaining states in $\mathbf{x}(t)$. Thus $n_{\text{ETI}} \geq n_w + n_k$. Note that all sets and matrices including \mathcal{O} , and P_G are relabeled accordingly. This reordering is only to simplify the exposition.

We are now ready to state our first key contribution: overapproximating the avoid set without tracking error. The following theorem overapproximates the continuous-time BRS of an obstacle and intersects it with the discrete-time reach-set of the PWA planning model to identify unsafe plans.

Theorem 11 (Avoid set w/o Tracking Error). *Consider the obstacle \mathcal{O}_i , some time $t \in \{0, \Delta t, \dots, t_f - \Delta t\}$, and some mode sequence $S = (s_0, \dots, s_t, s_{t+\Delta t}, \dots, s_{t_f-\Delta t})$. Suppose we compute the $(t_f - t)$ -time BRS $\bar{\Omega}_t$ as in (22). Let $A = \mathcal{B}(\text{proj}_{1:n_{\text{ETI}}}(\mathcal{O}_i) \times \mathbb{R}^{n_{\text{other}}}, \mathbf{C}_{s_t,t}, \mathbf{d}_{s_t,t})$, and define the intermediate avoid set $\bar{\Lambda}_{i,t,t} \subset \bar{\Omega}_t$ as:*

$$\bar{\Lambda}_{i,t,t} = \text{conv}(\text{proj}_{1:n_{\text{ETI}}}(A) \times X_{\text{other}}, \mathcal{O}_i) \cap \bar{\Omega}_t \quad (28)$$

Then, for any $\mathbf{x}(t) \in \bar{\Omega}_t \setminus \bar{\Lambda}_{i,t,t}$, $\mathbf{x}(t + \Delta t) = \mathbf{C}_{s_t,t} \mathbf{x}(t) + \mathbf{d}_{s_t,t}$,

$$\{\mathbf{x}(t) + \gamma(\mathbf{x}(t + \Delta t) - \mathbf{x}(t)) \mid 0 \leq \gamma \leq 1\} \cap \mathcal{O}_i = \emptyset. \quad (29)$$

Proof. See Appendix D. \square

In summary, Proposition 9 establishes a necessary condition for the collision to occur between two discrete timesteps, while Theorem 11 overapproximates the avoid sets contained in each intermediate BRS.

We now propose a straightforward scheme to construct the avoid set using Proposition 9 and Theorem 11: reference trajectories generated from outside the avoid set are guaranteed to avoid the obstacle. First, for each timestep $t = 0, \Delta t, \dots, t_f - \Delta t$ and for each obstacle $i = 1, \dots, n_{\mathcal{O}}$, we check if (24) is true; this reduces conservativeness because we identify obstacles for which we do not have to compute the avoid set $\bar{\Lambda}_{i,t,t}$ with Theorem 11, at the expense of additional convex hull computations. That is, one can speed up computation but potentially make the avoid set more conservative by skipping checking (24). Then, we apply the following corollary:

Corollary 12 (Avoid Set Computation). *We compute the avoid set $\bar{\Lambda}_{i,t,0}$ by computing the t -time BRS of $\bar{\Lambda}_{i,t,t}$. Mathematically,*

$$\bar{\Lambda}_{i,t,j} = \mathcal{B}(\bar{\Lambda}_{i,t,j+\Delta t}, \mathbf{C}_{s_{j,j}}, \mathbf{d}_{s_{j,j}}) \quad \forall j = 0, \Delta t, \dots, t - \Delta t. \quad (30)$$

Then, the final, overapproximated avoid set $\bar{\Lambda}$ can be stored as a union of H -polytopes as:

$$\bar{\Lambda} = \bigcup_{i=1}^{n_{\mathcal{O}}} \bigcup_{t=0}^{t_f-\Delta t} \mathbb{1}_{(24)}(i, t, \bar{\Lambda}_{i,t,0}), \quad (31)$$

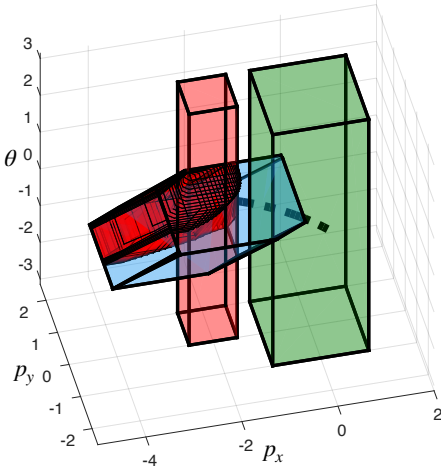


Fig. 3: Visualization of the reach set (blue) and the avoid set (red) from Section IV-C for the TurtleBot example (Section III-D and Fig. 2), with an obstacle (light red), extended to all $\theta \in [-\pi, \pi]$. The expert plan used to compute the reach set is shown as a dashed black line; notice that it intersects the obstacle. However, PARC is still able to compute the reach set (blue) and thereby find plans that safely reach the goal set (green).

where the set indicator function $\mathbb{1}_{(24)}(\cdot, \cdot, \cdot) : \mathbb{N} \times \mathbb{R} \times X \rightarrow X$ returns its input if (24) is true for corresponding (i, t) , or returns \emptyset if otherwise.

Proof. This follows as a consequence of Theorem 11 and since the BRS operation, \mathcal{B} is exact for an affine system defined for a mode sequence (Lemma 1). \square

To sample from within the reach set but not from the avoid set, one can either rejection-sample, sample via random-walk algorithms [34], [35], or compute the set difference between the reach set and the avoid set [36], and then sample via solving an LP. The reach set and the avoid set are shown in Fig. 3; notice that the avoid set is a nonconvex union of polytopes.

D. Estimating Tracking Error

Now that we have a basis for computing the BRAS, we will model tracking error such that, when incorporated into the PARC framework, we can produce plans that, *when followed by the tracking model*, guaranteed to reach the goal region while avoiding all obstacles.

Our method is based on [10], [37]. We sample $(\mathbf{z}_{0,j}, \mathbf{k}_j) \in \tilde{Z} \times \tilde{K} \subset Z \times K$ for $j = 1, \dots, n_{\text{sample}}$ uniformly, where $\tilde{Z} \times \tilde{K}$ is a hyperrectangle created by partitioning $Z \times K$; we do not index this partition to ease notation. We then have the robot start at $\mathbf{z}_{0,j}$ to track the plans parameterized by initial planning state $\mathbf{p}_{0,j} \triangleq (\mathbf{z}_{0,j})_{1:n_p}$ and trajectory parameter \mathbf{k}_j , and compute the error between the planned and realized trajectories in the workspace states (recall that we assume the goal and obstacles are subsets of workspace).

We consider two types of errors: the *maximum final error* $e_{t_f, i} \in \mathbb{R}$ for goal-reaching, and *maximum interval error* $\tilde{e}_{t, i} \in \mathbb{R}$ for obstacle avoidance, defined for the discrete-time at time t and the i^{th} dimension of \mathbf{z} and \mathbf{p} . PARC require two types of errors because it provides continuous-time guarantees for

obstacle avoidance, but gives guarantees at the final timestep only for goal-reaching.

For each workspace coordinate $i = 1, \dots, n_w$, we define the maximum final error $e_{t_f, i}$ as:

$$e_{t_f, i} = \max_j |\mathbf{p}_i(t_f; \mathbf{p}_{0,j}, \mathbf{k}_j) - \mathbf{z}_i(t_f; \mathbf{z}_{0,j}, \mathbf{k}_j)|, \quad (32)$$

where $\mathbf{p}_i(\cdot)$ and $\mathbf{z}_i(\cdot)$ are the i^{th} element of $\mathbf{p}(\cdot)$ and $\mathbf{z}(\cdot)$. In plain words, $e_{t_f, i}$ represents the maximum error observed at the final time t_f for the i^{th} workspace dimension.

For $t = 0, \Delta t, \dots, t_f - \Delta t$, $i = 1, \dots, n_w$, we define the maximum interval error $\tilde{e}_{t, i}$ as:

$$\tilde{e}_{t, i} = \max_{j, t' \in [t, t+\Delta t]} |\mathbf{p}_i(t'; \mathbf{p}_{0,j}, \mathbf{k}_j) - \mathbf{z}_i(t'; \mathbf{z}_{0,j}, \mathbf{k}_j)| \quad (33)$$

which is the maximum error observed *between* each discrete timestep for the i^{th} workspace dimension.

We assume this approach provides an upper bound for feasible tracking error, which can be proven for simple planning models [10], [37].

Assumption 13 (Maximum Sampled Error Contains Maximum Error). *We assume that, for a large enough n_{sample} ,*

$$e_{t_f, i} \geq \max_{\mathbf{z}_0 \in \tilde{Z}, \mathbf{k} \in \tilde{K}} |\mathbf{p}_i(t_f; \mathbf{p}_0, \mathbf{k}) - \mathbf{z}_i(t_f; \mathbf{z}_0, \mathbf{k})|, \quad (34a)$$

$$\tilde{e}_{t, i} \geq \max_{\mathbf{z}_0 \in \tilde{Z}, \mathbf{k} \in \tilde{K}, t' \in [t, t+\Delta t]} |\mathbf{p}_i(t'; \mathbf{p}_0, \mathbf{k}) - \mathbf{z}_i(t'; \mathbf{z}_0, \mathbf{k})|, \quad (34b)$$

for all $t = 0, \Delta t, \dots, t_f - \Delta t$, where $\mathbf{p}_0 = (\mathbf{z}_0)_{1:n_p}$.

This assumption is clearly a potential weakness of the method, but we find that it holds in practice because the sampling process produces adversarial $(\mathbf{z}_0, \mathbf{k})$ pairs. Furthermore, we can refine the tracking error estimate by increasing the fineness of the partition of $Z \times K$ into subsets $\tilde{Z} \times \tilde{K}$ [10].

To incorporate these errors into the geometric computation of PARC, we express them as the *maximum final error set* $E_{t_f} \subset \mathbb{R}^{n_x}$ and the *maximum interval error set* $\tilde{E}_t \subset \mathbb{R}^{n_x}$:

$$E_{t_f} = [-e_{t_f, 1}, e_{t_f, 1}] \times \dots \times [-e_{t_f, n_w}, e_{t_f, n_w}] \times \underbrace{\{0\} \times \dots \times \{0\}}_{(n_{p_{\text{other}}} + n_k) \text{ times}}, \quad (35)$$

$$\tilde{E}_t = [-\tilde{e}_{t, 1}, \tilde{e}_{t, 1}] \times \dots \times [-\tilde{e}_{t, n_w}, \tilde{e}_{t, n_w}] \times \underbrace{\{0\} \times \dots \times \{0\}}_{(n_{p_{\text{other}}} + n_k) \text{ times}}. \quad (36)$$

It is straightforward to express these intervals as H-polytopes [22]. The Cartesian product with empty sets is necessary to augment the states for Minkowski sum and Pontryagin difference operations with the obstacles and the goal.

An example of computed tracking error for a near-hover quadrotor dynamical model is shown in Fig. 8.

E. Incorporating Tracking Error into PARC

To conclude our proposed method, we incorporate tracking error into PARC's BRAS computation, thereby transferring guarantees for the planning model to the tracking model. In short, we get reach-avoid guarantees that incorporate tracking error by simply Minkowski summing the error with obstacles and Pontryagin differencing from the goal set.

1) *PARC: Reach Set with Tracking Error*: From Assumption 13, we assume the sampled tracking error is valid only over the compact hyperrectangle $\tilde{Z} \times \tilde{K}$. Thus, we must define a valid input region $\tilde{X} \subset X$ for which the computed reach set will have guarantees over:

$$\tilde{X} = \text{proj}_{1:n_w}(\tilde{Z}) \times \tilde{K} \times \text{proj}_{(n_w+1):n_p}(\tilde{Z}). \quad (37)$$

The projection and Cartesian product are necessary to reorder \tilde{Z} and \tilde{K} into that of (17).

To incorporate tracking error, we first tighten our assumption on the expert plan to find a mode sequence:

Assumption 14 (Expert Plan with Tracking Error). *We assume that a goal-reaching initial condition \mathbf{x}_0 that defines an expert plan is known and given for the PWA planning model in Section IV-A. Particularly, \mathbf{x}_0 is any point that satisfies:*

$$\psi(\mathbf{x}_0) \in P_G \ominus E_{t_f}. \quad (38)$$

Intuitively, $E_{t_f,i}$ captures the maximum tracking error at time t_f : if the plans can arrive at the smaller goal region $P_G \ominus E_{t_f}$, then the robot should be guaranteed to arrive at the original, bigger goal region P_G at time t_f .

With a given expert plan, we can obtain \mathbf{x}_0 's mode sequence using (21), then compute the underapproximated reach set Ω_0 of the goal similar to Proposition 8.

Proposition 15 (Reach Set with Tracking Error). *Consider a mode sequence $S = (s_0, \dots, s_{t_f-\Delta t})$. Then we can underapproximate the reach set Ω_0 corresponding to this mode sequence by:*

$$\Omega_{t_f} = P_G \ominus E_{t_f}, \quad (39a)$$

$$\Omega_t = \mathcal{B}(\overline{\Omega}_{t+\Delta t}, \mathbf{C}_{s_t,t}, \mathbf{d}_{s_t,t}) \quad \forall t = \Delta t, \dots, t_f - \Delta t, \quad (39b)$$

$$\Omega_0 = \mathcal{B}(\overline{\Omega}_{\Delta t}, \mathbf{C}_{s_{\Delta t},\Delta t}, \mathbf{d}_{s_{\Delta t},\Delta t}) \cap \tilde{X}, \quad (39c)$$

Proof. This follows from Lemma 1, Assumption 13, and Proposition 8. \square

This extends Proposition 8 by shrinking the goal set and intersection with the tracking error data coverage domain to include tracking error. With Ω_0 computed, if the robot tracks any plan generated from an initial condition within Ω_0 , it is guaranteed to reach the goal at time t_f , but may not be safe; next we guarantee safety by computing the avoid set.

2) *PARC: Avoid Set with Tracking Error*: Consider the obstacle \mathcal{O}_i and some time $t \in \{0, \Delta t, \dots, t_f - \Delta t\}$. We define the i^{th} buffered obstacle $\tilde{\mathcal{O}}_{t,i}$ between time t and $t + \Delta t$ as:

$$\tilde{\mathcal{O}}_{t,i} = \mathcal{O}_i \oplus \tilde{E}_t. \quad (40)$$

Assuming \tilde{E}_t captures the maximum tracking error from t to $t + \Delta t$, by buffering \mathcal{O}_i with \tilde{E}_t , if the trajectory does not collide with $\tilde{\mathcal{O}}_{t,i}$, then the robot following the trajectory should never collide with $\mathcal{O}_{t,i}$. Thus, incorporating tracking errors into the PARC formulation for avoid set follows closely to that of Section IV-C, but with $\tilde{\mathcal{O}}_{t,i}$ instead of $\mathcal{O}_{t,i}$ as an obstacle.

Proposition 16 (Unsafe Plans w/ Tracking Error). *Consider the buffered obstacle $\tilde{\mathcal{O}}_{t,i}$ for some time $t \in \{0, \Delta t, \dots, t_f - \Delta t\}$, and the mode sequence $S = (s_0, \dots, s_t, s_{t+\Delta t}, \dots, s_{t_f-\Delta t})$. Compute the $(t_f - t)$ -time BRS Ω_t and the $(t_f - t - \Delta t)$ -time BRS $\Omega_{t+\Delta t}$ using (39). If any planning trajectories between Ω_t and $\Omega_{t+\Delta t}$ collide with $\tilde{\mathcal{O}}_{t,i}$, that is, if $\exists \mathbf{x}(t) \in \Omega_t, \mathbf{x}(t + \Delta t) = \mathbf{C}_{s_t,t}\mathbf{x}(t) + \mathbf{d}_{s_t,t} \in \Omega_{t+\Delta t}$ such that*

$$\tilde{\mathcal{O}}_{t,i} \cap \{\mathbf{x}(t) + \gamma(\mathbf{x}(t + \Delta t) - \mathbf{x}(t)) \mid 0 \leq \gamma \leq 1\} \neq \emptyset, \quad (41)$$

then

$$\tilde{\mathcal{O}}_{t,i} \cap \text{conv}(\Omega_t, \Omega_{t+\Delta t}) \neq \emptyset. \quad (42)$$

Proof. Follows from Propositions 15 and Proposition 9. \square

Finally, we can state our second key contribution: overapproximating the avoid set with tracking error (i.e., computing the BRAS).

Theorem 17 (Avoid set w/ Tracking Error). *Consider the buffered obstacle $\tilde{\mathcal{O}}_{t,i}$ for some time $t \in \{0, \Delta t, \dots, t_f - \Delta t\}$, and from (39), the $(t_f - t)$ -time BRS Ω_t of the mode sequence $S = (s_0, \dots, s_t, s_{t+\Delta t}, \dots, s_{t_f-\Delta t})$. Let $A = \mathcal{B}(\text{proj}_{1:n_{\text{ETI}}}(\tilde{\mathcal{O}}_{t,i}) \times \mathbb{R}^{n_{\text{other}}}, \mathbf{C}_{s_t,t}, \mathbf{d}_{s_t,t})$. Define the intermediate avoid set $\Lambda_{i,t} \subset \Omega_t$ as:*

$$\Lambda_{i,t} = \text{conv}(\text{proj}_{1:n_{\text{ETI}}}(A) \times X_{\text{other}}, \tilde{\mathcal{O}}_{t,i}) \cap \Omega_t. \quad (43)$$

Then, for any $\mathbf{x}(t) \in \Omega_t \setminus \Lambda_{i,t}$, $\mathbf{x}(t + \Delta t) = \mathbf{C}_{s_t,t}\mathbf{x}(t) + \mathbf{d}_{s_t,t}$,

$$\{\mathbf{x}(t) + \gamma(\mathbf{x}(t + \Delta t) - \mathbf{x}(t)) \mid 0 \leq \gamma \leq 1\} \cap \tilde{\mathcal{O}}_{t,i} = \emptyset. \quad (44)$$

Proof. Follows from Proposition 16 and Theorem 11. \square

We can adapt Corollary 12 to compute the avoid set $\Lambda_{i,t,0}$ by computing the t -time BRS of $\Lambda_{i,t,t}$ as

$$\Lambda_{i,t,j} = \mathcal{B}(\Lambda_{i,t,j+1}, \mathbf{C}_{s_j,j}, \mathbf{d}_{s_j,j}) \quad \forall j = 0, \Delta t, \dots, t - \Delta t. \quad (45)$$

Then, the final overapproximated avoid set Λ can be stored as a union of H-polytopes as:

$$\Lambda = \bigcup_{i=1}^{n_{\mathcal{O}}} \bigcup_{t=0}^{t_f-\Delta t} \mathbb{1}_{(42)}(i, t, \Lambda_{i,t,0}). \quad (46)$$

With the avoid set and the reach set from Section IV-E.1 computed, if the robot tracks any plans starting in $\Omega_0 \setminus \Lambda$ it is guaranteed to reach the goal region while avoiding all obstacles. Thus, the set $\Omega_0 \setminus \Lambda$ is the desired object BRAS $(t_f, \overline{P_G}, \overline{\mathcal{O}})$. Next, we demonstrate PARC's BRAS computation on a variety of numerical examples.

V. EXPERIMENTS

We now assess the utility of our proposed PARC method for generating safe trajectory plans near danger. We seek to understand the impact of planning model design (Section V-A), cooperative vs. adversarial planner-trackers (Section V-B), and tight approximation of planning model reachable sets (Section V-C). We also assess the utility of learning-based reach-avoid in Sections V-A and V-B.

Key result: PARC outperforms other methods in goal reaching, safety, and computation time, but requires careful choice of planning model.

To ensure fair assessment, we apply PARC to robots from the safe motion planning and control literature: a near-hover quadrotor in 2-D [15] and 3-D [5], and a more general quadrotor model in 3-D [10]. Implementation details are reported in Appendix E. All experiments, and training of learning-based methods, are run on a desktop computer with a 24 core i9 CPU, 32 GB RAM, and an Nvidia RTX 4090 GPU.

A. Impact of Planning Model Design

This experiment seeks to understand the impact of choosing a planning model for a given tracking model. We deploy PARC on a tracking model and environment that have been successfully solved by a Neural CLBF [15] approach.

To examine the importance of the planning model, we employ the *same dynamics* for both the planning and tracking model, namely 2-D near-hover quadrotor dynamics:

$$\dot{\mathbf{p}} = \dot{\mathbf{z}} = \frac{d}{dt} \begin{bmatrix} p_x \\ p_z \\ \theta \\ v_x \\ v_z \\ \omega \end{bmatrix} = \begin{bmatrix} v_x \\ v_z \\ \omega \\ \frac{1}{m} \sin(\theta)(F_l + F_r) \\ \frac{1}{m} \cos(\theta)(F_l + F_r) - g \\ \frac{1}{I} (F_l - F_r) \end{bmatrix} \quad (47)$$

The workspace states are $\mathbf{w} = [p_x \ p_y]^\top$, and the inputs are left- and right-side propeller forces

$$\mathbf{u} = \mathbf{k} = [F_l \ F_r]^\top,$$

which are held constant for $[0, t_f]$ to generate plans. The feedback controller \mathbf{u}_{fb} produces time-varying left- and right-side propeller forces using an iLQR controller [31].

The gravitational constant is $g = 9.81 \text{ m/s}^2$. The quadrotor's physical parameters $[I, m, r]$ are obtained from [15].

1) *Experiment Setup*: We use the obstacle and goal environment from [15, Sec. 6.3], wherein the quadrotor must navigate over an obstacle and through a small gap to a goal region (see the left side of Fig. 4 and Fig. 5).

We use PARC to compute a BRAS for this scenario with an expert plan, accounting and without accounting for tracking error. The planning model piece-wise affine (47) with 80 PWA regions, timestep $\Delta t = 0.1$ sec, and final time $t_f = 2$ sec. We assess the computation time, as well as the size of the BRAS to investigate the impact of planning model design.

2) *Hypothesis*: We expect PARC to be able to compute plans to the goal reliably, with no safety violations during $[0, t_f]$. However, due to the naïve choice of planning model, we expect the avoid set to be overly conservative, especially since (47) has three non-ETI states (v_x, v_z, ω) in its PWA formulation.

3) *Results*: Fig. 5 and Fig. 4 show PARC's attempt to construct a BRAS with and without accounting for tracking error. Surprisingly, despite the high-dimensional planning model, PARC only took 5.08 sec to compute the BRAS with tracking error and 4.62 sec without. By contrast, the Neural CLBF takes 3 hrs to train. After accounting for tracking error, PARC was no longer able to compute trajectories traveling

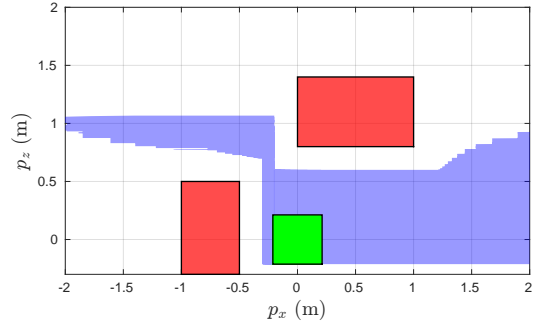


Fig. 4: Results of PARC on a naïve choice of planning model, without accounting for tracking error. Green indicates the goal region, red indicates the obstacles with the volume of the drone accounted for, and blue shows the reach set set-differenced with the avoid set without tracking error. Safe trajectories were successfully generated from the left of the leftmost obstacle.

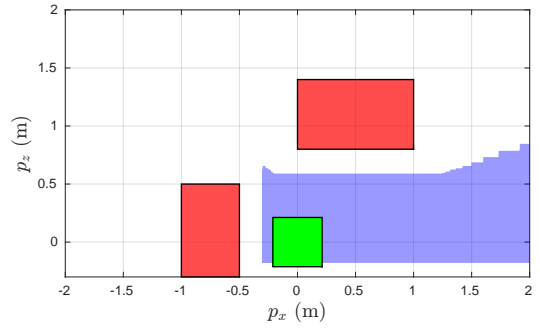


Fig. 5: Results of PARC on a naïve choice of planning model after accounting for tracking error. Green indicates the goal region, red indicates the obstacles with the volume of the drone accounted for, and blue shows the computed BRAS. There were no longer any safe trajectories generating from the left of the leftmost obstacle, which the Neural CLBF was able to accomplish.

from the left of the leftmost obstacle. No crashes or failure to goal-reach were reported when the tracking agent followed the trajectories generated from within the BRAS.

4) *Discussion*: The decrease in BRAS volume was expected due to the many non-ETI states, leading to over-conservativeness in avoid set computation. Moreover, as the problem framework requires the trajectory parameters F_l, F_r to be constant, the quadrotor shall continue accelerating after reaching the goal region, leading to instability should F_l, F_r be tracked.

In Appendix G and the next few examples, we show how a careful design of the planning model would lead to much better performance on more complicated scenarios, as well as enable stabilizing behavior such as braking without explicitly modeling velocity as a goal state.

B. Impact of Planner-Tracker Cooperation

We now study cooperative vs. adversarial planning and tracking models. We also further study the Neural CLBF [15] learning-based reach-avoid approach. For this experiment, we use a 3D near-hover quadrotor introduced for FaSTrack [5], a reachability-based planner tracker that uses adversarial planning and tracking models.

1) *Experiment Setup:* The tracking model and PARC’s planning model are listed in Appendix E. The quadrotor must navigate a narrow gap (width 1.8 m, compared to drone width 0.5 m) to reach its goal as shown in Fig. 7. We simulate 8,100 trials from different initial conditions. We measure the number of trials that reach the goal, and the number that crashes. We also consider the total computation time of each method.

2) *Hypotheses:* We anticipate that our PARC planner always reaches the goal safely. We also anticipate faster computation time of our reachability analysis versus the other two approaches, but note that FaSTrack does not need to recompute the reachable set for every obstacle. Since FaSTrack provides formal proof of safety, we anticipate it has no crashes. However, since it treats the planner and tracker as adversarial, we expect it to struggle to reach the goal. On the other hand, since CLBFs specifically balance safety and liveness, we expect it to reach the goal more often than FaSTrack but at the expense of crashing due to the high chance of learning an incorrect representation of safety when forced to operate near obstacles.

3) *Results:* Fig. 7 illustrates results for all methods with an initial position of $[4, -1, 3]^T$. FaSTrack (orange) fails to find a feasible plan that reaches the goal, the trajectory rolled out by Neural CLBF (magenta) violates safety, while the trajectory rolled out by PARC (blue) finds a plan that reaches the goal safely despite tracking error.

Fig. 6 illustrates the trajectories simulated on the grid of 8,100 initial positions using each method. Neural CLBF finds 576 successful positions (7.1 %), while safety is violated for the rest. FaSTrack finds 0 successful trajectories but never violates safety. However, PARC finds the plan to reach the goal without collision for 2,592 initial states (32 %).

FaSTrack takes 1 hr to compute its Tracking Error Bound (TEB) (which only needs to be done once offline). CLBF training took 5 hrs for this obstacle configuration. PARC computes the BRAS in 6.34 sec for this obstacle configuration.

4) *Discussion:* The performance of FaSTrack is notably compromised by the large, conservatively computed TEB, specified as a $2.47 \times 2.47 \times 0.1$ cuboid. This often results in the inability to compute feasible plans in spaces tighter than the TEB. However, as seen in the Fig. 8, sampled tracking error under parameterized plan, the tracking error is much smaller than TEB, enabling PARC to find a plan in challenging scenarios.

Although Neural CLBF succeeds in capturing most of the safe, unsafe, goal regions, the synthesized control policy steers some of the initial states to violate safety. Thus, the learning-based method sacrifices guarantees.

PARC has a strong safety guarantee, so every plan PARC found did not collide with the obstacles. We note that a better choice of planning model could increase PARC’s success rate; the simplicity of the single-integrator planning model, employed mainly for fair comparison with FaSTrack, reduced the flexibility of possible plans. Indeed we leverage a better choice of trajectory model next.

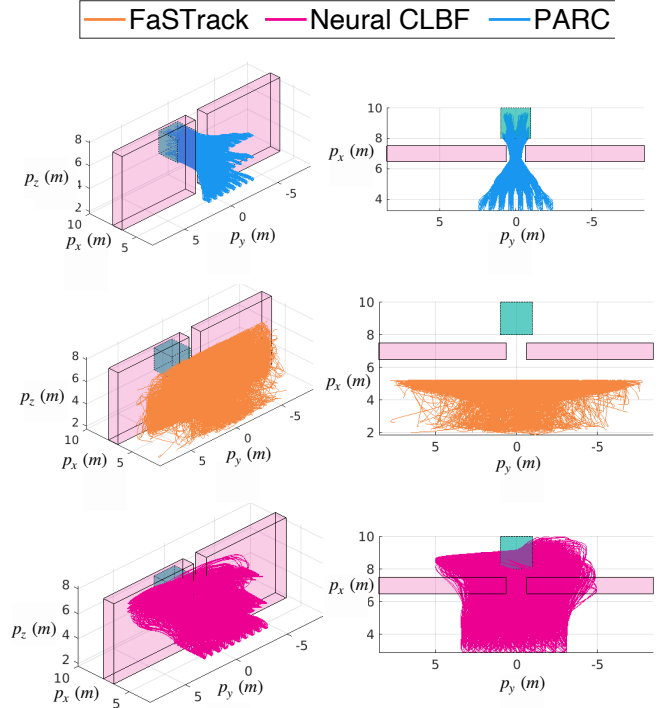


Fig. 6: Simulated trajectories of 10D quadrotor for 8,100 initial states using three methods: PARC, FaSTrack [5], Neural CLBF [15]. The green cuboid is the goal set and the pink cuboids are obstacles.

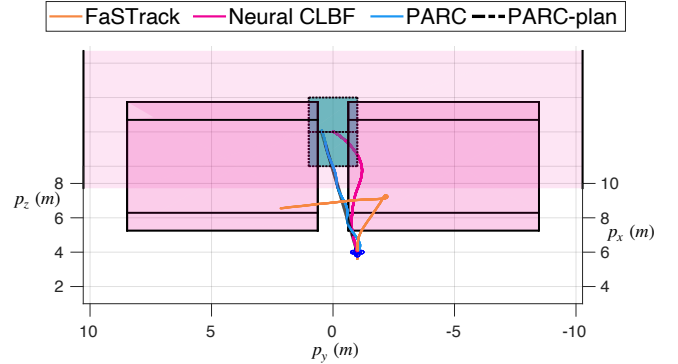


Fig. 7: Realized trajectory of the 10D quadrotor in the environment for 10 seconds using three methods: ours (blue), FaSTrack [5] (orange), Neural CLBF [15] (magenta). The black dashed line denotes the plan computed using PARC. The goal is represented as a green cube while the obstacle is magenta cuboids. The boundary of environments exist although not illustrated in the figure.

C. Impact of Tight Approximation for Planning Reachability

Finally, we seek to understand the importance of computing a tighter approximation of reachable set for the planning model. To do this, we compare against RTD implemented on a general 3-D quadrotor [10] using zonotope reachability [23]. This allows us to use the same tracking error model but employs a different approach to planning model reachability analysis.

1) *Experiment Setup:* Our experimental setup is similar to that of Section V-B but with a narrower gap.

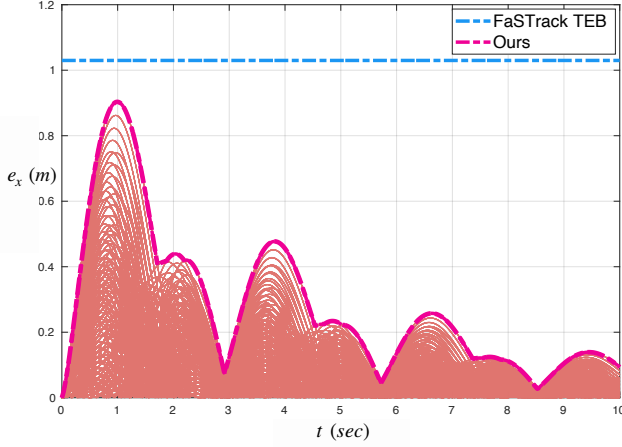


Fig. 8: Comparison of tracking error function between Fastrack and PARC for planning horizon $t_f = 10$ sec. FaSTrack computes a fixed, worst-case tracking error bound for all time because it assumes an adversarial planner, whereas PARC takes advantage of the smaller, time-varying tracking error that results from a planner and controller working together. The pale pink trajectories are samples used to compute the error as in Section IV-D.

We use the same planning model as quadrotor RTD [10], which generates time-varying polynomial positions in 3-D [38] with $\Delta t = 0.02$ sec with $t_f = 3$ sec; this formulation is affine time-varying in the trajectory parameters with no non-ETI states, so reachability can be tightly approximated by PARC. Both PARC and RTD use the same tracking error that is precomputed in [10].

The quadrotor is initialized in front of the narrow gap, directly facing the goal. It only receives information about the obstacles at this time (i.e., PARC cannot precompute the BARS). We give both methods 30 sec to attempt to find a trajectory to the goal through the gap. Note that RTD is focused on fast, safe replanning, so we let it attempt to replan as often as possible.

We declare success if the quadrotor reaches the goal region within 30 seconds without colliding with any obstacles.

2) *Hypothesis*: We anticipate that PARC will always safely find a way to reach the goal since we know the narrow gap is large enough to do so, and PARC’s primary source of conservativeness is its tracking error estimation (which is identical to that of RTD). We anticipate that RTD will reach the goal much less often because it suffers an additional course of conservativeness from using an approximate method to compute the reachable set of its planning model.

3) *Results*: A visual comparison of RTD and PARC is shown in Fig. 9. PARC was able to compute the BRAS (i.e., a continuum of safe motion plans) in 15.4 sec and thereby reach the goal; after BARS computation, PARC generated 308 safe plans in 0.046 sec by uniform sampling. On the other hand, RTD was not able to reach the goal at all, despite frequently replanning an average of every 51ms. RTD eventually became stuck after flying too close to one obstacle (but not colliding). Neither method had any collisions.

4) *Discussion*: As expected, both RTD and PARC guaranteed safety. However, only PARC was able to traverse

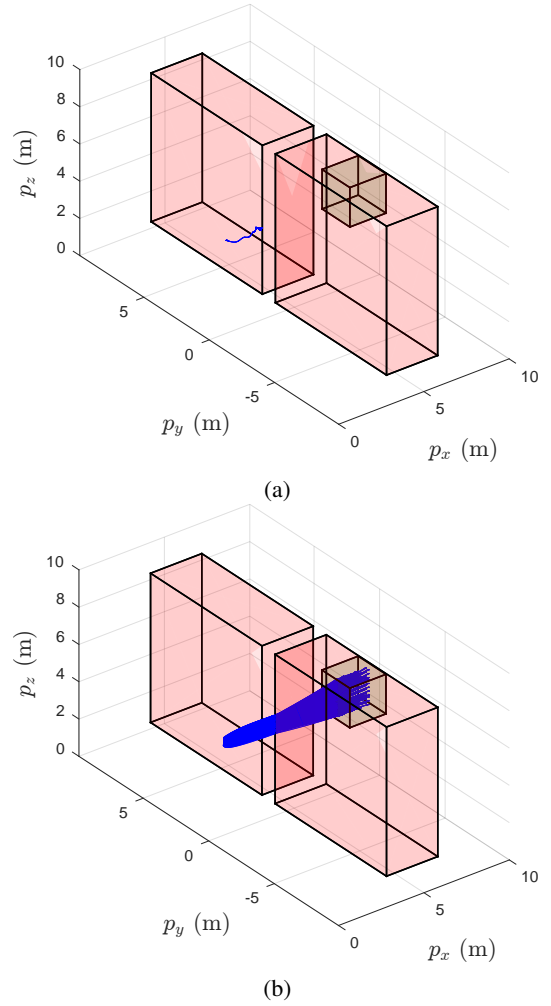


Fig. 9: Experiment with general quadrotor model in 3-D using RTD in (a) and PARC in (b). The red boxes are the obstacle and the green cube is the goal set; the green sphere shows the center of the goal used as a cost function for RTD. RTD’s overall trajectory after 30 sec of replanning is shown in blue, unable to reach the goal. PARC generates the set of initial conditions that all produce *guaranteed* safe plans that reach the goal and avoids the obstacles. We sample PARC’s BRAS to find 308 safe trajectories (including tracking error), shown in blue.

through the narrow gap. Thus, this example clearly illustrates the utility of PARC’s tightly approximating reachable set computation in comparison to RTD’s approximation. Although PARC is significantly slower in planning when compared to RTD, once a BRAS is computed, the robot obtains a continuum of safe plans.

The main slowdown of PARC’s computation comes from the avoid set computation in (28) and (45), whose computation time increases quadratically with the number of time steps. In this example, we chose the small timesteps of 0.02 sec over the planning horizon of 3 sec for a fair comparison with RTD. But if a faster computation time is preferred over a finer trajectory model with potentially less tracking error, one can decrease the number of timesteps when defining the PWA system. Furthermore, our PARC implementation is not yet parallelized, which may lead to further speedups.

D. Overall Discussion

Through the above experiments, we have shown how our proposed PARC approach confers advantages in computing and using Backward Reach-Avoid Set (BRAS). By careful use of PWA systems, plus bounded tracking error, we are able to generate safe motion plans in cases where other methods are either too conservative or fail to compute entirely.

However, PARC still has room for improvement. Most obviously, the safe plan computation time is on the order of seconds for just a few obstacles; this is too slow for real-time operation. Furthermore, the planning model requires careful hand-crafting as shown in our experiments.

VI. DRIFT VEHICLE DEMONSTRATION

We now demonstrate the utility of PARC in safely planning extreme near-danger vehicle drifting maneuvers, where the robot loses controllability.

Key result: PARC enables computation of provably safe drift parking trajectories for the first time, extending the state of the art.

A. Background

1) *Drifting*: Drifting is when a vehicle turns with a high sideslip angle, causing tire saturation and losing direct control of its heading [39]. Stable drifting can be achieved by finding “drift equilibria” with constant yaw rate and sideslip angle of the highly nonlinear dynamics [39]–[42]. Drift parking, however, remains challenging due to the highly coupled inputs [43] and reduced controllability as the vehicle specifically must not maintain a drift equilibrium [44].

2) *Reach-Avoid Method Comparison*: To the best of our knowledge, no other method can guarantee safety and liveness for drift parking.

Our drifting tracking model dynamics (see (83) below) are not control affine, so directly applying a CBF or CLBF control approach is not tractable [45], [46]; future work may apply results for non-control-affine systems [47], [48]. Note, [15] poses a control affine vehicle dynamics model but does not include tire saturation, so cannot drift. Furthermore, our planning and tracking models are too high-dimensional for standard HJB value function computation [5], [49]; future work will compare against learning-based HJB [13]. The most similar work is RTD [9], [50], which has not been applied to these extreme dynamics. As a future implementation, RTD’s reachable set can use PARC’s formulation to enable a direct drifting comparison; then, the only difference with PARC is that RTD implicitly represents the avoid set. Due to this similarity, we focus on demonstrating PARC’s capabilities as opposed to a head-to-head comparison.

B. Demo Details

Extensive details are presented in Appendix H. Here, we briefly present setup, simulation results, and a discussion.

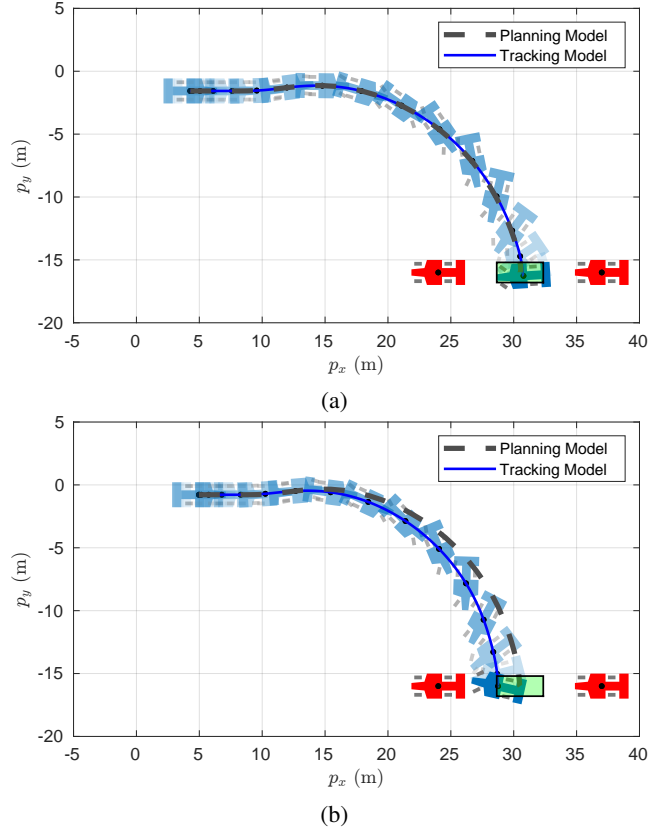


Fig. 10: Example planned drifting trajectories sampled from the Backward Reach-Avoid Set using PARC. The two red cars are obstacles. The goal set for the center of mass is in green. The trajectory with a very low tracking error is shown in (a), whereas a high tracking error is shown in (b). Critically *neither* collide with the obstacles, and both are represented in the single BRAS.

1) *Planning and Tracking Models*: As we saw in Section V-A, carefully planning model design is critical to PARC’s reach-avoid. In this case, we fit an affine time-varying model to drifting data collected by rolling out open-loop drifting maneuvers. This not only guarantees a reasonable planning model (i.e., it successfully parameterizes drifting maneuvers) but also demonstrates the flexibility of using PWA models for PARC since they can readily be learned from expert demonstrations.

We use a tracking model based on [39], [40], [42], [51], detailed in Appendix H. Our tracking controller is based on [51]: we first use nonlinear MPC to bring the car into a drifting state, then switch to open-loop control to complete the parking action (since the vehicle loses controllability when sliding sideways to a stop).

2) *Environment and Demo Setup*: The objective of this demo is to drift safely into a parallel parked state between two closely parked cars, as shown in Fig. 1 and Fig. 10. Our environment is inspired by a real-world demo video [52].

We assess PARC’s ability to compute the BRAS for this maneuver. We further evaluate safety trajectory rollouts using initial conditions and trajectory parameters sampled from the BRAS to check for collision.

3) *Results*: PARC’s computed BRAS for drift parking is shown in Fig. 1b. The BRAS took 5.52 sec to compute. We see that with the chosen controller and learned planning model, every choice of pair of initial planning state and trajectory parameter in the BRAS results in safely drift-parking the car. Fig. 10a and Fig. 10b show the best and worst case tracking error; in either case, since we sample from the BRAS, the vehicle satisfies both safety and goal-reaching.

4) *Discussion*: This demo showcased (i) PARC’s capability to generate safe and goal-reaching trajectories with challenging near-danger tasks such as reach-avoid drift parking, and (ii) the flexibility of PARC in terms of handling a suitable planning model from data. We notice that the BRAS is relatively small (see Fig. 1b) in the state space, indicating that drift parking is indeed a difficult maneuver. This emphasizes the importance of PARC minimizing conservativeness in the BRAS computation. However, it also suggests that this maneuver is brittle to large changes in initial conditions, and PARC will struggle to find drifting maneuvers for different goal sets or obstacle configurations. In future work, we plan to test more robust drifting controllers to produce a larger BRAS. With that in mind, our ultimate goal is physical hardware experiments on a platform such as the F1:10 car in Fig. 12.

VII. CONCLUSION

This paper has presented an approach to use Piecewise Affine Reach-avoid Computation (PARC) for safe goal-reaching robot trajectory planning near danger. PARC enables goal-reaching through narrow gaps and in tight obstacle configurations, even with extreme dynamics. The method outperforms a variety of state-of-the-art reach-avoid methods and establishes a new benchmark for safe, extreme vehicle motion planning. Future work will improve PARC’s computation time,

Limitations. PARC has several key limitations. First and foremost, it requires an assumption that the data coverage of sampled tracking error is large enough. While this assumption holds in practice (over hundreds of collision-free trials planned in this paper), it means that further mathematical work is necessary for true safety guarantees. Second, although PARC is faster than compared methods, it is still too slow for real-time; the present implementation has not been parallelized and may benefit from alternative representations to H-polytopes. Third, PARC has only been compared on hand-crafted examples of goal reaching near danger, and only in simulation. It is critical to validate the method across randomly-generated, realistic environments, on real hardware. To this end, the authors are preparing a small robotic car to perform hardware experiments in the coming months.

REFERENCES

- [1] J. F. Fisac, M. Chen, C. J. Tomlin, and S. S. Sastry, “Reach-avoid problems with time-varying dynamics, targets and constraints,” in *Proceedings of the 18th international conference on hybrid systems: computation and control*, 2015, pp. 11–20.
- [2] B. Alpern and F. B. Schneider, “Defining liveness,” *Information processing letters*, vol. 21, no. 4, pp. 181–185, 1985.
- [3] K. P. Wabersich, A. J. Taylor, J. J. Choi, et al., “Data-driven safety filters: Hamilton-jacobi reachability, control barrier functions, and predictive methods for uncertain systems,” *IEEE Control Systems Magazine*, vol. 43, no. 5, pp. 137–177, 2023.
- [4] K.-C. Hsu, H. Hu, and J. F. Fisac, “The safety filter: A unified view of safety-critical control in autonomous systems,” *arXiv preprint arXiv:2309.05837*, 2023.
- [5] M. Chen, S. L. Herbert, H. Hu, et al., “Fastrack: a modular framework for real-time motion planning and guaranteed safe tracking,” *IEEE Transactions on Automatic Control*, vol. 66, no. 12, pp. 5861–5876, 2021.
- [6] K. Garg, R. K. Cosner, U. Rosolia, A. D. Ames, and D. Panagou, “Multi-rate control design under input constraints via fixed-time barrier functions,” *IEEE Control Systems Letters*, vol. 6, pp. 608–613, 2021.
- [7] A. Majumdar and R. Tedrake, “Funnel libraries for real-time robust feedback motion planning,” *The International Journal of Robotics Research*, vol. 36, no. 8, pp. 947–982, 2017.
- [8] R. Tedrake, I. R. Manchester, M. Tobenkin, and J. W. Roberts, “LQR-trees: Feedback motion planning via sums-of-squares verification,” *The International Journal of Robotics Research*, vol. 29, no. 8, pp. 1038–1052, 2010.
- [9] S. Kousik, S. Vaskov, F. Bu, M. Johnson-Roberson, and R. Vasudevan, “Bridging the gap between safety and real-time performance in receding-horizon trajectory design for mobile robots,” *The International Journal of Robotics Research*, vol. 39, no. 12, pp. 1419–1469, 2020.
- [10] S. Kousik, P. Holmes, and R. Vasudevan, “Safe, aggressive quadrotor flight via reachability-based trajectory design,” in *Dynamic Systems and Control Conference*, American Society of Mechanical Engineers, vol. 59162, 2019, V003T19A010.
- [11] B. Landry, M. Chen, S. Hemley, and M. Pavone, “Reach-avoid problems via sum-of-squares optimization and dynamic programming,” in *2018 IEEE/RSJ International Conference on Intelligent Robots and Systems (IROS)*, IEEE, 2018, pp. 4325–4332.
- [12] M. Althoff, G. Frehse, and A. Girard, “Set propagation techniques for reachability analysis,” *Annual Review of Control, Robotics, and Autonomous Systems*, vol. 4, pp. 369–395, 2021.
- [13] S. Bansal and C. J. Tomlin, “Deepreach: A deep learning approach to high-dimensional reachability,” in *2021 IEEE International Conference on Robotics and Automation (ICRA)*, IEEE, 2021, pp. 1817–1824.
- [14] J. Michaux, Q. Chen, Y. Kwon, and R. Vasudevan, “Reachability-based Trajectory Design with Neural Implicit Safety Constraints,” *arXiv preprint arXiv:2302.07352*, 2023.
- [15] C. Dawson, Z. Qin, S. Gao, and C. Fan, “Safe nonlinear control using robust neural lyapunov-barrier functions,” in *Conference on Robot Learning*, PMLR, 2022, pp. 1724–1735.
- [16] W. Xiao, T.-H. Wang, R. Hasani, et al., “Barriernet: Differentiable control barrier functions for learning of safe robot control,” *IEEE Transactions on Robotics*, 2023.
- [17] M. Selim, A. Alanwar, S. Kousik, G. Gao, M. Pavone, and K. H. Johansson, “Safe reinforcement learning using black-box reachability analysis,” *IEEE Robotics and Automation Letters*, vol. 7, no. 4, pp. 10 665–10 672, 2022.
- [18] F. Christophersen, *Optimal Control of Constrained Piecewise Affine Systems* (Lecture Notes in Control and Information Sciences). Springer Berlin Heidelberg, 2007.
- [19] J. Thomas, S. Olaru, J. Buisson, and D. Dumur, “Robust model predictive control for piecewise affine systems subject to bounded disturbances,” *IFAC Proceedings Volumes*, vol. 39, no. 5, pp. 329–334, 2006.
- [20] E. C. Kerrigan and D. Q. Mayne, “Optimal control of constrained, piecewise affine systems with bounded disturbances,” in *Proceedings of the 41st IEEE Conference on Decision and Control*, 2002., IEEE, vol. 2, 2002, pp. 1552–1557.
- [21] S. V. Rakovic and D. Q. Mayne, “Robust time optimal obstacle avoidance problem for constrained discrete time systems,” in *Proceedings of the 44th IEEE Conference on Decision and Control*, IEEE, 2005, pp. 981–986.
- [22] M. Herceg, M. Kvasnica, C. N. Jones, and M. Morari, “Multi-parametric toolbox 3.0,” in *2013 European control conference (ECC)*, IEEE, 2013, pp. 502–510.

- [23] M. Althoff, "An Introduction to CORA 2015," *ARCH@ CPSWeek*, vol. 34, pp. 120–151, 2015.
- [24] R. Desimani and M. Prandini, "Robust constrained control of piecewise affine systems through set-based reachability computations," *International Journal of Robust and Nonlinear Control*, vol. 30, no. 15, pp. 5989–6020, 2020.
- [25] P. M. Wensing, M. Posa, Y. Hu, A. Escande, N. Mansard, and A. Del Prete, "Optimization-based control for dynamic legged robots," *IEEE Transactions on Robotics*, 2023.
- [26] J. A. Vincent and M. Schwager, "Reachable polyhedral marching (rpm): A safety verification algorithm for robotic systems with deep neural network components," in *2021 IEEE International Conference on Robotics and Automation (ICRA)*, IEEE, 2021, pp. 9029–9035.
- [27] J. K. Scott, D. M. Raimondo, G. R. Marseglia, and R. D. Braatz, "Constrained zonotopes: A new tool for set-based estimation and fault detection," *Automatica*, vol. 69, pp. 126–136, 2016.
- [28] D. Heß, M. Althoff, and T. Sattel, "Formal verification of maneuver automata for parameterized motion primitives," in *2014 IEEE/RSJ International Conference on Intelligent Robots and Systems*, IEEE, 2014, pp. 1474–1481.
- [29] C. Grant, *Theory of Ordinary Differential Equations*. CreateSpace Independent Publishing Platform, 2014.
- [30] S. Vaskov, S. Kousik, H. Larson, et al., "Towards provably not-at-fault control of autonomous robots in arbitrary dynamic environments," *arXiv preprint arXiv:1902.02851*, 2019.
- [31] N. J. Kong, G. Council, and A. M. Johnson, "iLQR for piecewise-smooth hybrid dynamical systems," in *2021 60th IEEE Conference on Decision and Control (CDC)*, IEEE, 2021, pp. 5374–5381.
- [32] S. Casselman and L. Rodrigues, "A new methodology for piecewise affine models using Voronoi partitions," in *Proceedings of the 48th IEEE Conference on Decision and Control (CDC) held jointly with 2009 28th Chinese Control Conference*, IEEE, 2009, pp. 3920–3925.
- [33] R. Bonalli, A. Cauligi, A. Byland, and M. Pavone, "Gusto: Guaranteed sequential trajectory optimization via sequential convex programming," in *2019 International conference on robotics and automation (ICRA)*, IEEE, 2019, pp. 6741–6747.
- [34] R. Kannan and H. Narayanan, "Random walks on polytopes and an affine interior point method for linear programming," in *Proceedings of the forty-first annual ACM symposium on Theory of computing*, 2009, pp. 561–570.
- [35] Y. Chen, R. Dwivedi, M. J. Wainwright, and B. Yu, "Fast MCMC sampling algorithms on polytopes," *The Journal of Machine Learning Research*, vol. 19, no. 1, pp. 2146–2231, 2018.
- [36] M. Baotić, "Polytopic computations in constrained optimal control," *Automatika: časopis za automatiku, mjerenje, elektroniku, računarstvo i komunikacije*, vol. 50, no. 3-4, pp. 119–134, 2009.
- [37] Y. S. Shao, C. Chen, S. Kousik, and R. Vasudevan, "Reachability-based trajectory safeguard (RTS): A safe and fast reinforcement learning safety layer for continuous control," *IEEE Robotics and Automation Letters*, vol. 6, no. 2, pp. 3663–3670, 2021.
- [38] M. W. Mueller, M. Hehn, and R. D'Andrea, "A computationally efficient motion primitive for quadcopter trajectory generation," *IEEE transactions on robotics*, vol. 31, no. 6, pp. 1294–1310, 2015.
- [39] J. Y. Goh and J. C. Gerdes, "Simultaneous stabilization and tracking of basic automobile drifting trajectories," in *2016 IEEE Intelligent Vehicles Symposium (IV)*, IEEE, 2016, pp. 597–602.
- [40] J. Y. Goh, T. Goel, and J. Christian Gerdes, "Toward automated vehicle control beyond the stability limits: drifting along a general path," *Journal of Dynamic Systems, Measurement, and Control*, vol. 142, no. 2, p. 021 004, 2020.
- [41] T. Goel, J. Y. Goh, and J. C. Gerdes, "Opening new dimensions: Vehicle motion planning and control using brakes while drifting," in *2020 IEEE Intelligent Vehicles Symposium (IV)*, IEEE, 2020, pp. 560–565.
- [42] T. P. Weber and J. C. Gerdes, "Modeling and Control for Dynamic Drifting Trajectories," *IEEE Transactions on Intelligent Vehicles*, 2023.
- [43] B. Leng, Y. Yu, M. Liu, L. Cao, X. Yang, and L. Xiong, "Deep reinforcement learning-based drift parking control of automated vehicles," *Science China Technological Sciences*, vol. 66, no. 4, pp. 1152–1165, 2023.
- [44] J. Z. Kolter, C. Plagemann, D. T. Jackson, A. Y. Ng, and S. Thrun, "A probabilistic approach to mixed open-loop and closed-loop control, with application to extreme autonomous driving," in *2010 IEEE International Conference on Robotics and Automation*, IEEE, 2010, pp. 839–845.
- [45] A. D. Ames, X. Xu, J. W. Grizzle, and P. Tabuada, "Control barrier function based quadratic programs for safety critical systems," *IEEE Transactions on Automatic Control*, vol. 62, no. 8, pp. 3861–3876, 2016.
- [46] C. Dawson, S. Gao, and C. Fan, "Safe control with learned certificates: A survey of neural lyapunov, barrier, and contraction methods for robotics and control," *IEEE Transactions on Robotics*, 2023.
- [47] T. D. Son and Q. Nguyen, "Safety-critical control for non-affine nonlinear systems with application on autonomous vehicle," in *2019 IEEE 58th Conference on Decision and Control (CDC)*, IEEE, 2019, pp. 7623–7628.
- [48] J. Seo, J. Lee, E. Baek, R. Horowitz, and J. Choi, "Safety-critical control with nonaffine control inputs via a relaxed control barrier function for an autonomous vehicle," *IEEE Robotics and Automation Letters*, vol. 7, no. 2, pp. 1944–1951, 2022.
- [49] I. M. Mitchell, "The flexible, extensible and efficient toolbox of level set methods," *Journal of Scientific Computing*, vol. 35, pp. 300–329, 2008.
- [50] J. Liu, Y. Shao, L. Lymburner, et al., "Refine: Reachability-based trajectory design using robust feedback linearization and zonotopes," *arXiv preprint arXiv:2211.11997*, 2022.
- [51] E. Jelavic, J. Gonzales, and F. Borrelli, "Autonomous drift parking using a switched control strategy with onboard sensors," *IFAC-PapersOnLine*, vol. 50, no. 1, pp. 3714–3719, 2017.
- [52] Guinness World Records. "Tightest parallel park - guinness world records." [accessed Feb 1, 2024]. (2014). [Online]. Available: https://youtu.be/IRXW7Ne1_88.
- [53] A. Agrawal and K. Sreenath, "Discrete control barrier functions for safety-critical control of discrete systems with application to bipedal robot navigation," in *Robotics: Science and Systems*, Cambridge, MA, USA, vol. 13, 2017, pp. 1–10.
- [54] U. Rosolia, A. Singletary, and A. D. Ames, "Unified multirate control: From low-level actuation to high-level planning," *IEEE Transactions on Automatic Control*, vol. 67, no. 12, pp. 6627–6640, 2022.
- [55] F. Castaneda, J. J. Choi, W. Jung, B. Zhang, C. J. Tomlin, and K. Sreenath, "Probabilistic safe online learning with control barrier functions," *arXiv preprint arXiv:2208.10733*, 2022.
- [56] S. Herbert, J. J. Choi, S. Sanjeev, M. Gibson, K. Sreenath, and C. J. Tomlin, "Scalable learning of safety guarantees for autonomous systems using Hamilton-Jacobi reachability," in *2021 IEEE International Conference on Robotics and Automation (ICRA)*, IEEE, 2021, pp. 5914–5920.
- [57] H. Seo, D. Lee, C. Y. Son, I. Jang, C. J. Tomlin, and H. J. Kim, "Real-Time Robust Receding Horizon Planning Using Hamilton-Jacobi Reachability Analysis," *IEEE Transactions on Robotics*, vol. 39, no. 1, pp. 90–109, 2022.
- [58] S. V. Rakovic, B. Kouvaritakis, M. Cannon, C. Panos, and R. Findeisen, "Parameterized tube model predictive control," *IEEE Transactions on Automatic Control*, vol. 57, no. 11, pp. 2746–2761, 2012.
- [59] M. E. Villanueva, R. Quirynen, M. Diehl, B. Chachuat, and B. Houska, "Robust MPC via min-max differential inequalities," *Automatica*, vol. 77, pp. 311–321, 2017.
- [60] K. P. Wabersich and M. N. Zeilinger, "A predictive safety filter for learning-based control of constrained nonlinear dynamical systems," *Automatica*, vol. 129, p. 109 597, 2021.
- [61] T. Marcucci, M. Petersen, D. von Wrangel, and R. Tedrake, "Motion planning around obstacles with convex optimization," *Science robotics*, vol. 8, no. 84, ead7843, 2023.
- [62] T. Cohn, M. Petersen, M. Simchowitz, and R. Tedrake, "Non-Euclidean Motion Planning with Graphs of Geodesically-Convex Sets," *arXiv preprint arXiv:2305.06341*, 2023.
- [63] K.-C. Hsu, V. Rubies-Royo, C. J. Tomlin, and J. F. Fisac, "Safety and liveness guarantees through reach-avoid reinforcement learning," *arXiv preprint arXiv:2112.12288*, 2021.
- [64] O. So and C. Fan, "Solving Stabilize-Avoid Optimal Control via Epigraph Form and Deep Reinforcement Learning," *arXiv preprint arXiv:2305.14154*, 2023.

- [65] J. Borquez, K. Chakraborty, H. Wang, and S. Bansal, “On Safety and Liveness Filtering Using Hamilton-Jacobi Reachability Analysis,” *arXiv preprint arXiv:2312.15347*, 2023.
- [66] D. Fridovich-Keil, J. F. Fisac, and C. J. Tomlin, “Safely probabilistically complete real-time planning and exploration in unknown environments,” in *2019 International Conference on Robotics and Automation (ICRA)*, IEEE, 2019, pp. 7470–7476.
- [67] G. Williams, P. Drews, B. Goldfain, J. M. Rehg, and E. A. Theodorou, “Aggressive driving with model predictive path integral control,” in *2016 IEEE International Conference on Robotics and Automation (ICRA)*, IEEE, 2016, pp. 1433–1440.
- [68] K. Srinivasan, B. Eysenbach, S. Ha, J. Tan, and C. Finn, “Learning to be safe: Deep rl with a safety critic,” *arXiv preprint arXiv:2010.14603*, 2020.
- [69] K. P. Wabersich, L. Hewing, A. Carron, and M. N. Zeilinger, “Probabilistic model predictive safety certification for learning-based control,” *IEEE Transactions on Automatic Control*, vol. 67, no. 1, pp. 176–188, 2021.
- [70] J. Thumm and M. Althoff, “Provably safe deep reinforcement learning for robotic manipulation in human environments,” in *2022 International Conference on Robotics and Automation (ICRA)*, IEEE, 2022, pp. 6344–6350.
- [71] S. Singh, M. Chen, S. L. Herbert, C. J. Tomlin, and M. Pavone, “Robust tracking with model mismatch for fast and safe planning: an SOS optimization approach,” in *Algorithmic Foundations of Robotics XIII: Proceedings of the 13th Workshop on the Algorithmic Foundations of Robotics 13*, Springer, 2020, pp. 545–564.
- [72] M. Chen, S. Herbert, and C. J. Tomlin, “Fast reachable set approximations via state decoupling disturbances,” in *2016 IEEE 55th Conference on Decision and Control (CDC)*, IEEE, 2016, pp. 191–196.
- [73] S. Kousik, S. Vaskov, M. Johnson-Roberson, and R. Vasudevan, “Safe trajectory synthesis for autonomous driving in unforeseen environments,” in *Dynamic systems and control conference*, American Society of Mechanical Engineers, vol. 58271, 2017, V001T44A005.
- [74] E. Asarin, T. Dang, and A. Girard, “Hybridization methods for the analysis of nonlinear systems,” *Acta Informatica*, vol. 43, pp. 451–476, 2007.
- [75] T. Dang, O. Maler, and R. Testylier, “Accurate hybridization of nonlinear systems,” in *Proceedings of the 13th ACM international conference on Hybrid systems: computation and control*, 2010, pp. 11–20.
- [76] T. Marcucci, R. Deits, M. Gabiccini, A. Bicchi, and R. Tedrake, “Approximate hybrid model predictive control for multi-contact push recovery in complex environments,” in *2017 IEEE-RAS 17th international conference on humanoid robotics (Humanoids)*, IEEE, 2017, pp. 31–38.
- [77] N. Mehr, D. Sadigh, R. Horowitz, S. S. Sastry, and S. A. Seshia, “Stochastic predictive freeway ramp metering from signal temporal logic specifications,” in *2017 American Control Conference (ACC)*, IEEE, 2017, pp. 4884–4889.
- [78] S. Sadraddini and R. Tedrake, “Sampling-based polytopic trees for approximate optimal control of piecewise affine systems,” in *2019 International Conference on Robotics and Automation (ICRA)*, IEEE, 2019, pp. 7690–7696.
- [79] T. Marcucci and R. Tedrake, “Mixed-integer formulations for optimal control of piecewise-affine systems,” in *Proceedings of the 22nd ACM International Conference on Hybrid Systems: Computation and Control*, 2019, pp. 230–239.
- [80] V. Sakizlis, K. I. Kouramas, and E. N. Pistikopoulos, “Linear model predictive control via multiparametric programming,” *Multi-Parametric Model-Based Control: Volume 2: Theory and Applications*, pp. 1–23, 2007.
- [81] M. Baotic, “Optimal control of piecewise affine systems: A multiparametric approach,” Ph.D. dissertation, ETH Zurich, 2005.
- [82] K. Fukuda, “Cddlib reference manual,” *Report version 093a*, McGill University, Montréal, Quebec, Canada, 2003.
- [83] A. Maréchal, D. Monniaux, and M. Périn, “Scalable minimizing-operators on polyhedra via parametric linear programming,” in *Static Analysis: 24th International Symposium, SAS 2017, New York, NY, USA, August 30–September 1, 2017, Proceedings 24*, Springer, 2017, pp. 212–231.
- [84] S. P. Boyd and L. Vandenberghe, *Convex optimization*. Cambridge university press, 2004.
- [85] T. Lee, M. Leok, and N. H. McClamroch, “Control of complex maneuvers for a quadrotor UAV using geometric methods on SE (3),” *arXiv preprint arXiv:1003.2005*, 2010.
- [86] W. Dong, G.-Y. Gu, X. Zhu, and H. Ding, “Development of a quadrotor test bed—modelling, parameter identification, controller design and trajectory generation,” *International Journal of Advanced Robotic Systems*, vol. 12, no. 2, p. 7, 2015.
- [87] E. Fiala, *Lateral Forces at the Rolling Pneumatic Tire*. 1954.
- [88] T. K. Lau, “Learning autonomous drift parking from one demonstration,” in *2011 IEEE International Conference on Robotics and Biomimetics*, IEEE, 2011, pp. 1456–1461.
- [89] D. Nguyen-Tuong and J. Peters, “Model learning for robot control: a survey,” *Cognitive processing*, vol. 12, pp. 319–340, 2011.

APPENDIX

A. Related Work

We now discuss methods that guarantee safety (avoiding dangerous states) and liveness (reaching a goal) for control systems and robot motion planning. In particular, we discuss optimal control methods, safety filters, and planner-tracker frameworks. Then, we discuss piecewise affine (PWA) system models, which we leverage to overcome limitations of conservativeness and computational tractability for providing safety and liveness guarantees with state-of-the-art methods.

1) *Optimal Control Methods*: Many safety methods focus on synthesizing or analyzing controllers. There has been extensive development of techniques such as Control Barrier Functions (CBFs) [45], [53]–[55], Hamilton-Jacobi (HJ) reachability [56], [57], sums-of-squares reachability [7], [8], robust model predictive control (MPC) [58]–[60], and graphs of convex sets (GCS) [61], [62]. Yet, only a minority of these methods address the dual objectives of liveness and safety [63]–[66]. Some methods seek a balance between performance and safety by implicitly integrating each constraint into the cost function of optimal control problem, solved through methods like MPC [67] or reinforcement learning [68], but can fail to offer hard satisfaction of such constraints.

The key challenge with most optimal control methods is to synthesize a controller that accounts for arbitrary bounded disturbances to a model of a robot. By contrast, in this work, we seek to synthesize a planner that cooperates with, and leverages knowledge about, an imperfect controller.

2) *Safety Filters*: A related strategy prioritizes safety through the use of safety filters [3], [69]; indeed, many optimal control methods can also be cast as safety filters [4], [45], [53]. In this case, a performance-oriented controller is minimally altered by a safety-oriented controller when the system is *about to* violate the safety constraints, mostly building on the safe invariant sets. Since this approach prioritizes safety over performance, thereby enforcing the hard satisfaction of safety in any case, the safety filter might produce conservative behavior. One way to mitigate conservativeness is to leverage reinforcement learning to exploit the safety filter [37], [70].

The key challenge with safety filters is that they intervene at the control level, and typically treat upstream planning as a disturbance [5], [71]. This can severely impact liveness, because the planner and controller are treated as adversarial, as opposed to cooperative. By contrast, we adopt a cooperative framework.

Another notable challenge, which we do not address, is extending to systems with very high-dimensional states or input/observation spaces. While some traditional approaches have tried a divide-and-conquer approach for high dimensions [72], the most promising path forward appears to be learning-based methods [13]–[17]. However, by relying on deep or machine learning, these methods essentially lose all safety guarantees above 12-D. We look forward to potentially attacking high-dimensional systems by fusing our proposed method with learning in the future.

3) *Planner-Tracker Methods*: The final category of safe planning and control methods that we discuss is the *planner-tracker* framework [5], [9], [10], [14]. These methods use a simplified model to enable fast plan generation; plans are then tracked by a controller that uses a high-fidelity tracking model of a robot.

Two representative approaches are FaSTrack [5] and Reachability-Based Trajectory Design (RTD) [9], [10]. FaSTrack employs Hamilton-Jacobi (HJ) reachability to precompute a worst-case error bound between the planning and tracking models, then dilates obstacles by this bound to ensure safe planning online. RTD precomputes a forward reachable set (FRS) of a parameterized set of planning model trajectories and associated (time-varying) tracking error, then uses the FRS to find safe plans at runtime. We compare our proposed method against both FaSTrack and RTD.

The primary challenge for planner-tracker methods is that the computational advantage of the planning model comes at the cost of model discrepancy [5], [10], [71], [73]. An additional key challenge is that the numerical representation of safety can be overly conservative even when just representing the planning model and ignoring model error. In this work, we design a planner-tracker framework that *exactly* represents trajectories of the planning model using piecewise affine systems, meaning that we only need to account for model error. We find that this significantly reduces conservativeness over related methods.

4) *Piecewise-Affine Systems*: In this paper, we propose a parameterized, time-variant piecewise-affine (PWA) system as our planning model. PWA systems, which evolve through different affine models based on state regions (modes), adeptly capture nonlinear dynamics. Their capacity for modeling non-smooth dynamics through hybridization is well-documented [74], [75] and they are prevalently used to approximate complex nonlinear hybrid systems, including legged locomotion [76], traffic systems [77], and neural network [26].

However, planning with PWA systems, which involves solving their control problem, is recognized as challenging due to the necessity of determining both input and mode sequences [78]. Standard solutions, including mixed-integer convex programming (MICP) [79] and multiparametric programming [80], [81], face computational challenges, particularly with increasing time steps exacerbating the number of integer decision variables.

To handle this challenge, we take advantage of *mode sequences*; it is well-established that a known mode sequence

greatly simplifies computation [19]–[21]. By leveraging sampling to synthesize likely mode sequences, our proposed approach significantly improves computational efficiency to enable successful computation of reach-avoid motion plans.

B. Operations on H-Polytopes

The intersection of H-polytopes is an H-polytope:

$$\begin{aligned} \mathcal{P}(\mathbf{A}_1, \mathbf{b}_1) \cap \mathcal{P}(\mathbf{A}_2, \mathbf{b}_2) &= \{\mathbf{x} \mid \mathbf{A}_1 \mathbf{x} \leq \mathbf{b}_1, \mathbf{A}_2 \mathbf{x} \leq \mathbf{b}_2\}, \\ &= \mathcal{P}\left(\begin{bmatrix} \mathbf{A}_1 \\ \mathbf{A}_2 \end{bmatrix}, \begin{bmatrix} \mathbf{b}_1 \\ \mathbf{b}_2 \end{bmatrix}\right). \end{aligned} \quad (48)$$

The Minkowski sum \oplus is

$$P_1 \oplus P_2 = \{\mathbf{x} + \mathbf{y} \mid \mathbf{x} \in P_1, \mathbf{y} \in P_2\}, \quad (49)$$

which can be computed as one H-polytope by solving a linear program (LP) [22]. The Minkowski sum essentially adds a “buffer” to the object being summed, which we use to pad the obstacles to account for tracking error in our reachability analysis.

Similarly, the Pontryagin Difference \ominus is

$$P_1 \ominus P_2 = \{\mathbf{x} \in P_1 \mid \mathbf{x} + \mathbf{y} \in P_1 \ \forall \ \mathbf{y} \in P_2\}, \quad (50)$$

which can be expressed as one H-polytope by subtracting the support of P_2 for each inequality of P_1 [22]. This essentially inverts the Minkowski sum, reducing the volume of an H-polytope, which we use to shrink a goal set to account for tracking error.

The Cartesian product \times is exactly an H-polytope:

$$P_1 \times P_2 = \left\{ \begin{bmatrix} \mathbf{x} \\ \mathbf{y} \end{bmatrix} \mid \mathbf{x} \in \mathcal{P}(\mathbf{A}_1, \mathbf{b}_1), \mathbf{y} \in \mathcal{P}(\mathbf{A}_2, \mathbf{b}_2) \right\}, \quad (51a)$$

$$= \mathcal{P}\left(\begin{bmatrix} \mathbf{A}_1 & \mathbf{0} \\ \mathbf{0} & \mathbf{A}_2 \end{bmatrix}, \begin{bmatrix} \mathbf{b}_1 \\ \mathbf{b}_2 \end{bmatrix}\right). \quad (51b)$$

We use this to combine low-dimensional reachable sets into higher dimensions, and to ensure that H-polytopes have equal dimensions for operations such as Minkowski sums and Pontryagin differences.

The convex hull is

$$\text{conv}(P_1, P_2) = \{\mathbf{x} + \gamma(\mathbf{y} - \mathbf{x}) \mid 0 \leq \gamma \leq 1, \mathbf{x}, \mathbf{y} \in P_1 \cup P_2\}, \quad (52)$$

which can be computed as one H-polytope by vertex enumeration, computing the convex hull of the vertices, and expressing the result in H-polytope form [82]. The convex hull contains all straight lines between two sets, which we use to overapproximate trajectories between discrete time points to secure continuous time safety guarantees.

For an n -dimensional H-polytope $\mathcal{P}(\mathbf{A}, \mathbf{b})$, the projection from the p^{th} dimension to the q^{th} dimension for some $p \leq q \leq n$ is defined as:

$$\begin{aligned} \text{proj}_{p,q}(\mathcal{P}(\mathbf{A}, \mathbf{b})) &= \{[\mathbf{0}_a, \mathbf{I}_b, \mathbf{0}_c] \mathbf{x} \mid \mathbf{A} \mathbf{x} \leq \mathbf{b}\}, \quad \text{where} \\ a &= (q - p + 1) \times (p - 1), \\ b &= (q - p + 1) \text{ and} \\ c &= (q - p + 1) \times (n - q) \end{aligned} \quad (53)$$

The right-hand side of (53) is exactly an *AH-polytope*, which can be converted to an H-polytope using block elimination, Fourier-Motzkin elimination, parametric linear programming, or vertex enumeration [82], [83]. Somewhat the opposite of Cartesian product, the projection operation lowers the dimensions of the input polytope, which will be useful for retrieving low-dimensional information if only a subset of the original states is of interest.

Note that convex hull and projection are NP-hard for H-polytopes, exponentially scaling in computational time and complexity with the dimension of the polytope [12]. However, since PARC performs polytope computation only for low-dimensional (≤ 6 -D) planning models, the computational time and complexity remain reasonable, as shown in Section V.

C. Method for Affinizing a Nonlinear System

We convert a nonlinear system into a PWA system via sampling in its state space, then computing Voronoi regions and linearizing the dynamics in each region, similar to in [32]. In particular, we apply the following:

Proposition 18. *Express the domain X as a H-polytope $\mathcal{P}(\mathbf{A}_X, \mathbf{b}_X)$. Consider linearization points $\mathbf{x}_{t,i}^* \in X$, $i = 1, \dots, n_t^*$. Then for $i = 1, \dots, n_t^*$, the Voronoi cells $V_{i,t}$ given by*

$$V_{i,t} = \bar{V}_{i,t} \cap X, \quad (54a)$$

$$\bar{V}_{i,t} = \left\{ \mathbf{x} \mid \|\mathbf{x} - \mathbf{x}_{t,i}^*\|_2^2 \leq \|\mathbf{x} - \mathbf{x}_{t,j}^*\|_2^2, j = 1, \dots, n_t^* \right\}, \quad (54b)$$

are compact H-polytopes that fulfill (5), and can therefore be the PWA regions of a PWA system.

Proof. It was proven in [84] that $\bar{V}_{i,t}$ is a closed, but not necessarily bounded H-polytope. In fact,

$$\bar{V}_{i,t} = \left\{ \mathbf{x} \mid \begin{bmatrix} (\mathbf{x} - \mathbf{x}_{t,i}^*) \cdot (\mathbf{x} - \mathbf{x}_{t,i}^*) \\ \vdots \\ (\mathbf{x} - \mathbf{x}_{t,i}^*) \cdot (\mathbf{x} - \mathbf{x}_{t,i}^*) \end{bmatrix} \leq \begin{bmatrix} (\mathbf{x} - \mathbf{x}_{t,1}^*) \cdot (\mathbf{x} - \mathbf{x}_{t,1}^*) \\ \vdots \\ (\mathbf{x} - \mathbf{x}_{t,n^*(t)}^*) \cdot (\mathbf{x} - \mathbf{x}_{t,n^*(t)}^*) \end{bmatrix} \right\}, \quad (55a)$$

$$= \left\{ \mathbf{x} \mid \begin{bmatrix} (2\mathbf{x}_{t,1}^* - 2\mathbf{x}_{t,i}^*)^\top \\ \vdots \\ (2\mathbf{x}_{t,n^*(t)}^* - 2\mathbf{x}_{t,i}^*)^\top \end{bmatrix} \mathbf{x} \leq \begin{bmatrix} \|\mathbf{x}_{t,1}^*\|_2^2 - \|\mathbf{x}_{t,i}^*\|_2^2 \\ \vdots \\ \|\mathbf{x}_{t,n^*(t)}^*\|_2^2 - \|\mathbf{x}_{t,i}^*\|_2^2 \end{bmatrix} \right\}, \quad (55b)$$

$$= \mathcal{P} \left(\begin{bmatrix} (2\mathbf{x}_{t,1}^* - 2\mathbf{x}_{t,i}^*)^\top \\ \vdots \\ (2\mathbf{x}_{t,n^*(t)}^* - 2\mathbf{x}_{t,i}^*)^\top \end{bmatrix}, \begin{bmatrix} \|\mathbf{x}_{t,1}^*\|_2^2 - \|\mathbf{x}_{t,i}^*\|_2^2 \\ \vdots \\ \|\mathbf{x}_{t,n^*(t)}^*\|_2^2 - \|\mathbf{x}_{t,i}^*\|_2^2 \end{bmatrix} \right). \quad (55c)$$

Since H-polytopes are closed under intersection (as shown in (48)), and the intersection of a closed set and a compact set is compact, $V_{i,t}$ is a compact H-polytope from (54a).

Further, for any $i, j \in \{1, \dots, n_t^*\}$, $i \neq j$, the intersection of the interior of $V_{i,t}$ with $V_{j,t}$ is given by:

$$\begin{aligned} \text{int}(V_{i,t}) \cap V_{j,t} &= \left\{ \mathbf{x} \mid \|\mathbf{x} - \mathbf{x}_{t,i}^*\|_2^2 < \|\mathbf{x} - \mathbf{x}_{t,k}^*\|_2^2, \right. \\ &\quad \left. \|\mathbf{x} - \mathbf{x}_{t,j}^*\|_2^2 \leq \|\mathbf{x} - \mathbf{x}_{t,k}^*\|_2^2, k = 1, \dots, n_t^* \right\} \cap \text{int}(X), \end{aligned} \quad (56)$$

where $\text{int}(\cdot)$ is the interior of a set. However, notice that $\|\mathbf{x} - \mathbf{x}_{t,i}^*\|_2^2 < \|\mathbf{x} - \mathbf{x}_{t,k}^*\|_2^2$ and $\|\mathbf{x} - \mathbf{x}_{t,j}^*\|_2^2 \leq \|\mathbf{x} - \mathbf{x}_{t,k}^*\|_2^2$ for $k = 1, \dots, n_t^*(t)$ implies $\|\mathbf{x} - \mathbf{x}_{t,i}^*\|_2^2 < \|\mathbf{x} - \mathbf{x}_{t,j}^*\|_2^2$ and $\|\mathbf{x} - \mathbf{x}_{t,j}^*\|_2^2 \leq \|\mathbf{x} - \mathbf{x}_{t,i}^*\|_2^2$, which is impossible. Thus,

$$\text{int}(V_{i,t}) \cap V_{j,t} = \emptyset, \quad (57)$$

which is exactly the condition (5).

Therefore, $V_{i,t}$ defines the PWA regions of a PWA system, with each of the $n_{\text{PWA},t} = n_t^*$ regions given by:

$$\mathbf{A}_{i,t} = \begin{bmatrix} (2\mathbf{x}_{t,1}^* - 2\mathbf{x}_{t,i}^*)^\top \\ \vdots \\ (2\mathbf{x}_{t,n^*(t)}^* - 2\mathbf{x}_{t,i}^*)^\top \\ \mathbf{A}_X \end{bmatrix}, \quad (58)$$

$$\mathbf{b}_{i,t} = \begin{bmatrix} \|\mathbf{x}_{t,1}^*\|_2^2 - \|\mathbf{x}_{t,i}^*\|_2^2 \\ \vdots \\ \|\mathbf{x}_{t,n^*(t)}^*\|_2^2 - \|\mathbf{x}_{t,i}^*\|_2^2 \\ \mathbf{b}_X \end{bmatrix}, \quad (59)$$

for $i = 1, \dots, n_t^*$. \square

D. Proof of Theorem 11: Avoid Set without Tracking Error

Here, we prove Theorem 11, which is our paper's main result. We first introduce the notations used throughout the proof, then provide a concise proof sketch, before finally elaborating the detailed proof.

Proof. Notation. For clarity, we introduce the block matrix representation of $\mathbf{C}_{s_t,t} - \mathbf{I}_{n_x}$ and $\mathbf{d}_{s_t,t}$:

$$\mathbf{C}_{s_t,t} - \mathbf{I}_{n_x} \triangleq \begin{bmatrix} \mathbf{C}_1 & \mathbf{C}_2 \\ \mathbf{C}_3 & \mathbf{C}_4 \end{bmatrix}, \quad \mathbf{d}_{s_t,t} \triangleq \begin{bmatrix} \mathbf{d}_1 \\ \mathbf{d}_2 \end{bmatrix} \quad (60)$$

where

$$\begin{aligned} \mathbf{C}_1 &\in \mathbb{R}^{n_{x\text{ETI}} \times n_{x\text{ETI}}}, & \mathbf{C}_2 &\in \mathbb{R}^{n_{x\text{ETI}} \times n_{x\text{other}}}, \\ \mathbf{C}_3 &\in \mathbb{R}^{n_{x\text{other}} \times n_{x\text{ETI}}}, & \mathbf{C}_4 &\in \mathbb{R}^{n_{x\text{other}} \times n_{x\text{other}}}, \\ \mathbf{d}_1 &\in \mathbb{R}^{n_{x\text{ETI}}}, & \mathbf{d}_2 &\in \mathbb{R}^{n_{x\text{other}}}. \end{aligned}$$

We denote the projection of obstacle \mathcal{O}_i and $(t_f - t)$ -time BRS $\bar{\mathcal{O}}_t$ onto the subspace X_{ETI} by $\mathcal{O}_{\text{ETI}} \triangleq \text{proj}_{1:n_{x\text{ETI}}}(\mathcal{O}_i)$ and $\bar{\mathcal{O}}_{\text{ETI}} \triangleq \text{proj}_{1:n_{x\text{ETI}}}(\bar{\mathcal{O}}_t)$, respectively. Similarly, the projection of $\bar{\mathcal{O}}_t$ onto the subspace X_{other} is denoted as $\bar{\mathcal{O}}_{\text{other}}$. We also denote $\mathcal{O}_+ \triangleq \mathcal{O}_{\text{ETI}} \times \mathbb{R}^{n_{x\text{other}}}$ for brevity.

Proof sketch. We reinterpret the theorem as a set-inclusion problem between a *true avoid set* P and *over-approximated avoid set* $\bar{\Lambda}_{i,t,t}$. Then, a conservative avoid set Q is defined, from which we derive the sufficient condition for set-inclusion. Using the Extended-Translation-Invariance (ETI) assumption (Assumption 2) and Lemma 10, we prove the satisfaction of the sufficient condition.

Detailed Proof. We first define the true avoid set P , a set of states that satisfy the equation (28) as follows:

$$P = \{\mathbf{x} \in \bar{\Omega}_t \mid \exists (\hat{\mathbf{x}}, \gamma) \in \mathcal{O}_i \times [0, 1] \text{ s.t. } \mathbf{x} + \gamma(\mathbf{C}_{s_t,t}\mathbf{x} + \mathbf{d}_{s_t,t} - \mathbf{x}) = \hat{\mathbf{x}}\} \quad (61)$$

Note that the theorem holds if and only if $P \subset \bar{\Lambda}_{i,t,t}$.

Next, to derive the sufficient condition for $P \subset \bar{\Lambda}_{i,t,t}$, we define a *conservative* avoid set Q :

$$Q = \{\mathbf{x}_{\text{ETI}} \in \bar{\Omega}_{\text{ETI}} \mid \exists (\mathbf{x}_{\text{other}}, \hat{\mathbf{x}}_{\text{ETI}}, \gamma) \in \bar{\Omega}_{\text{other}} \times \mathcal{O}_{\text{ETI}} \times [0, 1] \text{ s.t. } \mathbf{x}_{\text{ETI}} + \gamma(\mathbf{C}_1\mathbf{x}_{\text{ETI}} + \mathbf{C}_2\mathbf{x}_{\text{other}} + \mathbf{d}_1) = \hat{\mathbf{x}}_{\text{ETI}}\} \quad (62)$$

Note that $\mathbf{x} = [\mathbf{x}_{\text{ETI}}^\top, \mathbf{x}_{\text{other}}^\top]^\top \in P$ implies $\mathbf{x}_{\text{ETI}} \in Q$, $\mathbf{x}_{\text{other}} \in X_{\text{other}}$, $\mathbf{x} \in \bar{\Omega}_t$, which leads to:

$$P \subset (Q \times X_{\text{other}}) \cap \bar{\Omega}_t \quad (63)$$

Building on this relation, we derive the sufficient condition for the theorem as follows:

$$Q \subset \text{conv}(\text{proj}_{1:n_{\text{ETI}}}(A), \mathcal{O}_{\text{ETI}}) \quad (64)$$

since satisfaction of (64) and (63) implies $P \subset \bar{\Lambda}_{i,t,t}$.

Now we prove the sufficient condition (64) using the ETI assumption. Fix $\hat{\mathbf{x}}_{\text{ETI}} \in Q$. Then by definition of Q , there exists $(\tilde{\mathbf{x}}_{\text{other}}, \tilde{\mathbf{x}}_{\text{ETI}}, \tilde{\gamma}) \in \bar{\Omega}_{\text{other}} \times \mathcal{O}_{\text{ETI}} \times [0, 1]$ that satisfies:

$$\tilde{\mathbf{x}}_{\text{ETI}} + \tilde{\gamma}(\mathbf{C}_1\tilde{\mathbf{x}}_{\text{ETI}} + \mathbf{C}_2\tilde{\mathbf{x}}_{\text{other}} + \mathbf{d}_1) = \hat{\mathbf{x}}_{\text{ETI}} \quad (65)$$

By rearranging the equation, we get:

$$\begin{aligned} \tilde{\mathbf{x}}_{\text{ETI}} &= \tilde{\gamma}(\hat{\mathbf{x}}_{\text{ETI}} - (\mathbf{C}_1\tilde{\mathbf{x}}_{\text{ETI}} + \mathbf{C}_2\tilde{\mathbf{x}}_{\text{other}} + \mathbf{d}_1)) + (1 - \tilde{\gamma})\hat{\mathbf{x}}_{\text{ETI}} \\ &= \tilde{\gamma}\mathbf{y} + (1 - \tilde{\gamma})\hat{\mathbf{x}}_{\text{ETI}} \end{aligned} \quad (66)$$

where noting $\hat{\mathbf{x}}_{\text{ETI}} \in \mathcal{O}_{\text{ETI}}$, it suffices to prove $\mathbf{y} \in \text{proj}_{1:n_{\text{ETI}}}(A) = \text{proj}_{1:n_{\text{ETI}}}(\mathcal{B}(\mathcal{O}_+, \mathbf{C}_{s_t,t}, \mathbf{d}_{s_t,t}))$ to prove (64). This is shown by proving $[\mathbf{y}^\top, \tilde{\mathbf{x}}_{\text{other}}^\top]^\top \in \mathcal{B}(\mathcal{O}_+, \mathbf{C}_{s_t,t}, \mathbf{d}_{s_t,t})$. Noting $\mathcal{O}_+ = \mathcal{O}_{\text{ETI}} \times \mathbb{R}^{n_{\text{other}}}$, we have to show

$$\mathbf{y} + \mathbf{C}_1\mathbf{y} + \mathbf{C}_2\tilde{\mathbf{x}}_{\text{other}} + \mathbf{d}_1 \in \mathcal{O}_{\text{ETI}} \quad (67)$$

$$\tilde{\mathbf{x}}_{\text{other}} + \mathbf{C}_3\mathbf{y} + \mathbf{C}_4\tilde{\mathbf{x}}_{\text{other}} + \mathbf{d}_2 \in \mathbb{R}^{n_{\text{other}}}. \quad (68)$$

Equation (68) is immediate, while (67) is true by

$$\mathbf{y} + \mathbf{C}_1\mathbf{y} + \mathbf{C}_2\tilde{\mathbf{x}}_{\text{other}} + \mathbf{d}_1 \quad (69)$$

$$\begin{aligned} &= \hat{\mathbf{x}}_{\text{ETI}} - (\mathbf{C}_1\hat{\mathbf{x}}_{\text{ETI}} + \mathbf{C}_2\tilde{\mathbf{x}}_{\text{other}} + \mathbf{d}_1) \\ &\quad + \mathbf{C}_1(\hat{\mathbf{x}}_{\text{ETI}} - (\mathbf{C}_1\hat{\mathbf{x}}_{\text{ETI}} + \mathbf{C}_2\tilde{\mathbf{x}}_{\text{other}} + \mathbf{d}_1)) \\ &\quad + \mathbf{C}_2\tilde{\mathbf{x}}_{\text{other}} + \mathbf{d}_1 \end{aligned} \quad (70)$$

$$= \hat{\mathbf{x}}_{\text{ETI}} - \mathbf{C}_1^2\hat{\mathbf{x}}_{\text{ETI}} - \mathbf{C}_1\mathbf{C}_2\tilde{\mathbf{x}}_{\text{other}} - \mathbf{C}_1\mathbf{d}_1 \quad (71)$$

$$= \hat{\mathbf{x}}_{\text{ETI}} - \mathbf{C}_1(\mathbf{C}_1\hat{\mathbf{x}}_{\text{ETI}} + \mathbf{C}_2\tilde{\mathbf{x}}_{\text{other}} + \mathbf{d}_1) \quad (72)$$

$$= \hat{\mathbf{x}}_{\text{ETI}} \in \mathcal{O}_{\text{ETI}} \quad (73)$$

The equation (73) follows from (72) using ETI Assumption 2 and the result of Lemma 10, namely:

$$\mathbf{C}_{X_{\text{ETI}}}(\mathbf{C}_{s_t,t}\mathbf{x} + \mathbf{d}_{s_t,t})_{1:n_{\text{ETI}}} = \mathbf{C}_1(\mathbf{C}_1\mathbf{x}_{\text{ETI}} + \mathbf{C}_2\mathbf{x}_{\text{other}} + \mathbf{d}_1) = 0 \quad \forall \mathbf{x} \in X \quad (74)$$

Since $\mathbf{y} \in \text{proj}_{1:n_{\text{ETI}}}(A)$ and $\hat{\mathbf{x}}_{\text{ETI}} \in \mathcal{O}_{\text{ETI}}$, by (66), $\tilde{\mathbf{x}}_{\text{ETI}} \in \text{conv}(\text{proj}_{1:n_{\text{ETI}}}(A), \mathcal{O}_{\text{ETI}})$. Hence the sufficient condition (64) is proved, and the theorem is proved accordingly. \square

E. Experiment Details

1) *Near-Hover Quadrotor in 3-D:* For the planning model, we employ the 3D single integrator, described as:

$$\begin{aligned} \dot{p}_x &= \hat{v}_x \\ \dot{p}_y &= \hat{v}_y \\ \dot{p}_z &= \hat{v}_z \end{aligned} \quad (75)$$

where the planning states $\mathbf{p} = [p_x, p_y, p_z]^\top$ represents the position of the robot, and trajectory parameter $\mathbf{k} = [\hat{v}_x, \hat{v}_y, \hat{v}_z]^\top$ denotes the desired velocity of the robot. The trajectory parameter domain is chosen to be $K = [-0.5, 0.5]^3$.

For the tracking model, we adopt a simplified 10-D quadrotor assuming near-hover conditions (i.e. small pitch and roll) [5], expressed by:

$$\begin{aligned} \dot{p}_x &= v_x \\ \dot{p}_y &= v_y \\ \dot{p}_z &= v_z \\ \dot{v}_x &= g \tan(\theta_x) \\ \dot{v}_y &= g \tan(\theta_y) \\ \dot{v}_z &= k_T \alpha_z - g \\ \dot{\theta}_x &= -d_1 \theta_x + \omega_x \\ \dot{\theta}_y &= -d_1 \theta_y + \omega_y \\ \dot{\omega}_x &= -d_0 \theta_x + n_0 \alpha_x \\ \dot{\omega}_y &= -d_0 \theta_y + n_0 \alpha_y \end{aligned} \quad (76)$$

where the states (p_x, p_y, p_z) denote the position, (v_x, v_y, v_z) are velocities, (θ_x, θ_y) are pitch and roll, and (ω_x, ω_y) are pitch and roll rates. The control input $\mathbf{u} = (\alpha_x, \alpha_y, \alpha_z)$ is the desired pitch and roll (α_x, α_y) and the vertical thrust α_z . The model parameters (d_0, d_1, n_0, k_T) and control input bound U are referenced from FaSTrack [5]. A simple Linear Quadratic Regulator (LQR) linearized around the tracking error $e = 0$ is employed for the feedback controller.

2) *General Quadrotor in 3-D:* We consider the time-switched polynomial planning model defined in [10], [38],

where, for $0 \leq t < t_{pk}$,

$$\dot{p}_x = \frac{c_1(k_{vx}, k_{ax}, k_{pkx})}{6} t^3 + \frac{c_2(k_{vx}, k_{ax}, k_{pkx})}{2} t^2 + k_{ax}t + k_{vx}, \quad (77a)$$

$$\dot{p}_y = \frac{c_1(k_{vy}, k_{ay}, k_{pky})}{6} t^3 + \frac{c_2(k_{vy}, k_{ay}, k_{pky})}{2} t^2 + k_{ay}t + k_{vy}, \quad (77b)$$

$$\dot{p}_z = \frac{c_1(k_{vz}, k_{az}, k_{pkz})}{6} t^3 + \frac{c_2(k_{vz}, k_{az}, k_{pkz})}{2} t^2 + k_{az}t + k_{vz}, \quad (77c)$$

$$c_1(k_v, k_a, k_{pk}) = \frac{12}{t_{pk}^3} k_v + \frac{6}{t_{pk}^2} k_a - \frac{12}{t_{pk}^3} k_{pk}, \quad (77d)$$

$$c_2(k_v, k_a, k_{pk}) = -\frac{6}{t_{pk}^2} k_v - \frac{4}{t_{pk}} k_a + \frac{6}{t_{pk}^2} k_{pk}, \quad (77e)$$

and for $t_{pk} \leq t \leq t_f$,

$$\dot{p}_x = \frac{c_3(k_{pkx})}{6} (t - t_{pk})^3 + \frac{c_4(k_{pkx})}{2} (t - t_{pk})^2 + k_{pkx}, \quad (78a)$$

$$\dot{p}_y = \frac{c_3(k_{pky})}{6} (t - t_{pk})^3 + \frac{c_4(k_{pky})}{2} (t - t_{pk})^2 + k_{pky}, \quad (78b)$$

$$\dot{p}_z = \frac{c_3(k_{pkz})}{6} (t - t_{pk})^3 + \frac{c_4(k_{pkz})}{2} (t - t_{pk})^2 + k_{pkz}, \quad (78c)$$

$$c_3(k_{pk}) = \frac{12}{(t_f - t_{pk})^3} k_{pk}, \quad (78d)$$

$$c_4(k_{pk}) = \frac{-6}{(t_f - t_{pk})^2} k_{pk}, \quad (78e)$$

where $t_f = 3$, $t_{pk} = 1$, the planning states and workspace $\mathbf{p} = \mathbf{w} = [p_x, p_y, p_z]^\top$ that represents the position of the quadrotor, and trajectory parameters $\mathbf{k} = [k_{vx}, k_{ax}, k_{pkx}, k_{vy}, k_{ay}, k_{pky}, k_{vz}, k_{az}, k_{pkz}]^\top$, where k_{vx}, k_{vy}, k_{vz} represents the desired initial speed, k_{ax}, k_{ay}, k_{az} represents the desired initial acceleration, and $k_{pkx}, k_{pky}, k_{pkz}$ represents the desired speed at $t = t_{pk}$.

This planning model can be separated into one low-dimensional model for each of the three workspace dimensions. That is, we can consider the planning states and workspace $\mathbf{p}_x = \mathbf{w}_x = p_x$ and trajectory parameters $\mathbf{k}_x = [k_{vx}, k_{ax}, k_{pkx}]$, defined by the dynamics (77a) and (78a), compute the reach set $\Omega_{0,x} \subset \mathbb{R}^4$ and avoid set $\Lambda_{i,t,0,x} \subset \mathbb{R}^4$ for each $t = 0, \Delta t, \dots, t_f - \Delta t$ and each $i = 1, \dots, n_\odot$ using PARC, and repeat for p_y and p_z .

We recover the 12-D reach set Ω_0 and avoid set Λ by:

$$\Omega_0 = \Omega_{0,x} \times \Omega_{0,y} \times \Omega_{0,z}, \quad (79)$$

$$\Lambda = \bigcup_{i=1}^{n_\odot} \bigcup_{t=0}^{t_f - \Delta t} \Lambda_{i,t,0,x} \times \Lambda_{i,t,0,y} \times \Lambda_{i,t,0,z}. \quad (80)$$

The tracking model for the system is from [10], [85],

defined as:

$$\begin{bmatrix} \dot{p}_x \\ \dot{p}_y \\ \dot{p}_z \end{bmatrix} = \mathbf{v}, \quad (81a)$$

$$\dot{\mathbf{v}} = \tau \mathbf{Re}_3 - m g \mathbf{e}_3, \quad (81b)$$

$$\dot{\boldsymbol{\omega}} = \mathbf{J}^{-1} \left(\begin{bmatrix} \mu_x \\ \mu_y \\ \mu_z \end{bmatrix} - \boldsymbol{\omega} \times \mathbf{J} \boldsymbol{\omega} \right), \quad (81c)$$

$$\dot{\mathbf{R}} = \mathbf{R} \text{hat}(\boldsymbol{\omega}), \quad (81d)$$

where $\mathbf{v} \in \mathbb{R}^3$ is velocity, $\mathbf{R} \in \text{SO}(3)$ is the attitude, $\mathbf{e}_3 \in \mathbb{R}^3$ is the unit vector in the inertial frame that points “up” relative to the ground, $m = 0.547$, $g = 9.81$, $\boldsymbol{\omega} \in \mathbb{R}^3$ is the angular velocity, $\mathbf{J} = \text{diag}(0.0033, 0.0033, 0.0058)$, $\text{hat} : \mathbb{R}^3 \rightarrow \text{SO}(3)$ is the hat map operator [85], and the control inputs $\mathbf{u} = [\tau, \mu_x, \mu_y, \mu_z]^\top$ are net thrust and body moments.

3) Comparison Methods:

a) *FaSTrack*: FaSTrack is a planner-tracker framework that precomputes a uniform Tracking Error Bound (TEB) (maximum possible tracking error) using Hamilton-Jacobi (HJ) reachability analysis. Obstacles are padded by the TEB; then, as long as the planner only plans outside the padded obstacles the robot is safe. During the TEB computation, FaSTrack also synthesizes a controller to guarantee the bound. We use RRT as the planning model as per [5].

b) *Neural CLBF*: Neural CLBF approximates a safety filter value function as a neural network, thereby segmenting the environment into goal, safe, and unsafe regions. The value function, trained with data from the entire state space, enables the generation of safe, goal-directed control inputs through Quadratic Programming (QP).

c) *Reachability-based Trajectory Design*: RTD is a planner-tracker framework that is very similar to PARC in that it uses a planner-tracker framework and compensates for tracking errors in a time-varying way. However, RTD leverages forward reachable sets (FRS). RTD numerically approximates the FRS either with sums-of-squares [9] or zonotope [10], [23] reachability. At runtime, RTD performs receding-horizon trajectory planning with nonlinear, nonconvex constraints derived from the FRS intersecting with obstacles to eliminate unsafe motion plans. Each parameterized plan contains a failsafe maneuver such that, if replanning fails, the previous (safe) maneuver can be executed.

F. Additional Experiment Details

1) Impact of Planner-Tracker Cooperation:

a) *Environment*: The environment is a $[0, 10] \times [-10, 10] \times [0, 10]$ cuboid (all lengths are in meters). The goal \overline{P}_G is a cube centered at $(p_x, p_y, p_z) = (9, 0, 5)$ with a side of 1 m. Obstacles $\overline{\mathcal{O}}$ include the floor, ceiling, and walls, and two additional cuboid obstacles of $[6.5, 7.5] \times [-8.2, -\Delta w/2] \times [0, 10]$ and $[6.5, 7.5] \times [\Delta w/2, 8.2] \times [0, 10]$ with varying Δw that denotes the gap between two obstacles. These are shown in Fig. 7 with a gap width $\Delta w = 1.8$. The obstacles are padded to accommodate the quadrotor’s body, approximated by a cuboid of $0.54 \times 0.54 \times 0.05$ using the specifications of

Hummingbird [86]. The planning horizon is $t_f = 10$ with time discretization $\Delta t = 0.1$ each. The frequency of the tracking controller is 1000Hz for all methods.

2) Impact of Tighter Planning Reachability:

a) *Environment*: The general 3-D quadrotor environment is similar to that of the 10-D near-hover quadrotor environment but with a narrower gap to the goal. The obstacles are defined as $\bar{\mathcal{O}}_1 = [3.23, 6.77] \times [0.23, 9.27] \times [0.73, 9.27]$, $\bar{\mathcal{O}}_2 = [3.23, 6.77] \times [-9.27, -0.23] \times [0.73, 9.27]$ (after accounting for an overapproximated volume of the quadrotor), that is, two walls with a clearance of 0.46, the goal region is defined as $\bar{\mathcal{P}}_G = [7.44, 9.56] \times [-1.06, 1.06] \times [3.94, 6.06]$, and the domains are defined as $P = [0, 10] \times [-10, 10] \times [0, 10]$ and $K = [-5.25, 5.25] \times [-10, 10] \times [-5.25, 5.25] \times [-5.25, 5.25] \times [-10, 10] \times [-5.25, 5.25] \times [-5.25, 5.25] \times [-10, 10] \times [-5.25, 5.25]$. The quadrotor starts stationary at $p_x = 1, p_y = 0, p_z = 5$. This means the quadrotor begins at the side of the wall opposite to the goal region, but the p_y coordinate is at the middle of the gap.

G. Additional Experiments

We provide a further comparison to the experiment in V-A by using a different planning model in the same environmental setting. The experiment seeks to show how PARC could improve using a better planning model under the same experimental conditions.

1) *Planning and Tracking Model*: We consider the time-switched polynomial model defined by (77a), (77c), (78a), and (78c), with $t_f = 2$, $t_{pk} = 1.5$, the planning states and workspace $\mathbf{p} = \mathbf{w} = [p_x, p_z]^T$, and trajectory parameters $\mathbf{k} = [k_{vx}, k_{ax}, k_{pkx}, k_{vz}, k_{az}, k_{pkz}]^T$. Just like in Section E.2, we separated the planning model into low-dimensional models for each of the two workspace dimensions, and recovered the high-dimensional reach set, avoid set, and BRAS by (79) and (80).

We used the same tracking model defined in (47) for a fair comparison.

2) *Experimental Setup*: Our experimental setup for the obstacles, goal region, and workspace domain are identical to that in Section V-A and [15]. We also use the same iLQR controlling scheme as in Section V-A but with the gains tuned to the new planning model. We define the domain for trajectory parameters with $K = [-1.5, 1.5] \times \{0\} \times [-0.1, 0.1] \times \{0\} \times [-1, 1] \times [-1.5, 1.5]$.

3) *Hypothesis*: We anticipate PARC to be able to compute a less conservative, but still guaranteed safe BRAS compared to Section V-A due to the reduced number (three vs. zero) of non-ETI states in the planning model. Moreover, we also expect PARC's computation time to be faster than the naïve model choice, as the dimension for polytopic computation has been reduced from 8 to 4.

Since the planning model in Appendix G.1 also incorporates stabilizing behavior for the quadrotor near the goal region [10], [38], we expect to produce similar reach-avoid results to [15], that is, the quadrotor would be able to safely navigate between the two obstacles while stopping at the goal region.

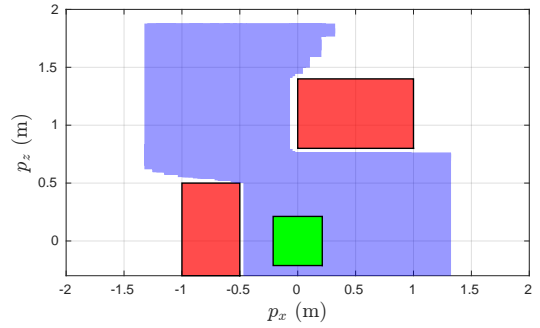


Fig. 11: Results of PARC on a time-switched polynomial planning model with stabilizing end-behavior, after accounting for tracking error. Green indicates the goal region, red indicates the obstacles with the volume of the drone accounted for, and blue shows the computed BRAS. Safe trajectories that pass between the two obstacles can now be generated compared to the results in Section V-A.

4) *Results*: Fig. 11 shows the BRAS constructed by PARC under the planning model in Appendix G.1. The BRAS computation took 1.47s, more than 3 times faster than that of the naïve model.

Trajectories were generated by uniformly sampling the BRAS. No crashes were reported, with the agent successfully *stopping* at the goal region in all simulations. Comparing Fig. 11 with Fig. 5, safe trajectories that travel in-between two obstacles can be generated, reproducing similar results to [15].

5) *Discussion*: The time-switched polynomial planning model has comparable tracking error with the naïve planning model in Section V-A. Thus, the reduced conservativeness in the computed BRAS for the polynomial model is largely due to the reduced number of non-ETI states in the PWA system, leading to a tighter approximation of the avoid sets. Note that the BRAS in Fig. 5 extends more to the right compared with Fig. 11 because the naïve planning model does not encode any stabilizing behavior, with the trajectory leading the agent to continuously accelerating towards the goal. Thus, within the same t_f , it was able to reach the goal from a further distance compared with the stabilizing trajectories.

We further note that, while the chosen domain for the time-switched polynomial planning model was not able to generate very parabolic trajectories that enable the agent to reach the goal from behind the left obstacle, this can be easily fixed by receding-horizon planning into the BRAS, or by performing PARC across multiple domains of trajectory parameters, both of which remains as future work.

In conclusion, these experiments show the importance of choosing a good planning model for PARC with minimal dimensions and non-ETI states without losing representation power in the trajectories. Should good planning models be unavailable, Section VI shows how one can construct planning models from data while using PARC to compute their corresponding BRAS.

H. Drift Vehicle Demo Details

We now define our tracking model, drift parking controller, and the time-variant affine planning model. We then present

results and a brief discussion.

1) *Tracking Model:* We use a tracking model based on [39], [40], [42], [51]:

$$\mathbf{z} = [p_x \ p_y \ \theta \ \omega \ v \ \beta]^\top \quad (82)$$

with its dynamics defined as:

$$\begin{aligned} \dot{p}_x &= v \cos(\theta + \beta) \\ \dot{p}_y &= v \sin(\theta + \beta) \\ \dot{\theta} &= \omega \\ \dot{\omega} &= \frac{1}{I_z} (L_a f_{y,f} \cos(\delta) + L_a f_{x,f} \sin(\delta) - L_b f_{y,r}) \\ \dot{v} &= \frac{1}{m} (f_{x,f} \cos(\delta - \beta) - f_{y,f} \sin(\delta - \beta) \\ &\quad + f_{x,r} \cos(\beta) + f_{y,r} \sin(\beta)) \\ \dot{\beta} &= \frac{1}{mv} (f_{x,f} \sin(\delta - \beta) - f_{y,f} \sin(\delta - \beta) \\ &\quad + f_{x,r} \cos(\beta) + f_{y,r} \sin(\beta)) - \omega \end{aligned} \quad (83)$$

In this single-track bicycle dynamics model, the first three states $p_x(m)$, $p_y(m)$, $\theta(\text{rad})$ describe the location of the car's center of mass and its orientation or yaw angle with respect to the stationary world frame. $\omega(\text{rad/s})$ is the yaw rate of the car; $v(\text{m/s})$ is the magnitude of the car's velocity measured from its center of mass. $\beta(\text{rad})$ is the sideslip angle between the car's traveling direction and its orientation.

The tracking model's control inputs are $\mathbf{u} = [f_{x,r}, \delta, f_{x,f, \max}]^\top$ which correspond to throttle (N), steering (rad), and brake (N). Note that $f_{x,r}$ only provides forces in the longitudinal direction of the rear tire. The brake only provides forces along the direction of the front tire. While its maximum value $f_{x,f, \max}$ is set by input, its actual magnitude $f_{x,f}$ is inversely proportional to the front tire frame longitudinal velocity. Such design ensures that the braking force goes to zero when the car stops moving.

The lateral forces on both the front and the rear tires,

$$f_{y,f} = f_{\text{front}}(\omega, v, \beta, f_{x,f}, \delta) \quad \text{and} \quad (84)$$

$$f_{y,r} = f_{\text{rear}}(\omega, v, \beta, f_{x,r}), \quad (85)$$

are formulated using the Fiala brush tire model [87]. Lastly, the car's physical parameters (I_z, m, L_a, L_b) as well as other constants used in the Fiala tire model are adopted from the DeLorean car specs from [39].

2) *Feedback Controller:* Literature in drift parking controllers falls into two categories. [43], [88] approached this problem with learning-based controllers. [44], [51] designed mixed open and closed-loop control strategies with the former using the probabilistic method and the latter deterministic.

In this demo, we adopt the control scheme described in [51]. We first used a nonlinear MPC tracking controller to bring the car into a drift state then switched to an open-loop control scheme to complete the drift parking action.

Specifically, given some initial state \mathbf{z}_0 and $\mathbf{k} = [v, \beta]^\top$, the controller provides input sequence $\mathbf{u}_{\text{fb}} = [f_{x,r}, \delta, f_{x,f, \max}]^\top$ for the tracking model such that the vehicle would be at

the appropriate sideslip angle to enter drifting regime at v . Next, as an open-loop PD controller continuously adjusts δ to maintain an increasing sideslip angle β , a one-time control input of $f_{x,r} = 0\text{N}$, $f_{x,f, \max} = 5163\text{N}$ (i.e., hard braking) is executed at the moment when β exceeds the planned β value (see \mathbf{k} in the planning model below).

3) *Planning Model:* Different from the experiment examples, the mixed open and closed loop drifting controller cannot track explicit trajectories when the car enters the drifting regime. Therefore, the construction of an analytical model that describes the entire drift parking trajectory is difficult or even impossible just like many robotics applications [89].

In this demo, we showcase the flexibility of PARC by constructing the planning model using data. We are directly constructing the planning model as a time-variant affine system with 3-D planning space and 2-D trajectory parameters, so PARC can be directly applied without Section IV-A. Specifically, we wish to design the affine dynamics in the form of:

$$\begin{bmatrix} p_{x,t+\Delta t} \\ p_{y,t+\Delta t} \\ \theta_{t+\Delta t} \\ v_{t+\Delta t} \\ \beta_{t+\Delta t} \end{bmatrix} = \begin{bmatrix} 1 & 0 & 0 & c_{vx,t} & c_{\beta x,t} \\ 0 & 1 & 0 & c_{vy,t} & c_{\beta y,t} \\ 0 & 0 & 1 & c_{v\theta,t} & c_{\beta\theta,t} \\ 0 & 0 & 0 & 1 & 0 \\ 0 & 0 & 0 & 0 & 1 \end{bmatrix} \begin{bmatrix} p_{x,t} \\ p_{y,t} \\ \theta_t \\ v_t \\ \beta_t \end{bmatrix} + \begin{bmatrix} d_{x,t} \\ d_{y,t} \\ d_{\theta,t} \\ 0 \\ 0 \end{bmatrix} \quad (86)$$

where the planning states $\mathbf{p} = [p_x, p_y, \theta]^\top$ are the world-frame coordinates and heading angle of the car, $\mathbf{w} = [p_x, p_y]^\top$ are the workspace states, trajectory parameters $\mathbf{k} = [v, \beta]^\top$ are the drifting velocity and the side-slip angle for controller switching, the domain for all timesteps of the PWA function is $P \times K$, and we wish to design $c_{vx,t}, c_{\beta x,t}, d_{x,t}, c_{vy,t}, c_{\beta y,t}, d_{y,t}, c_{v\theta,t}, c_{\beta\theta,t}$, and $d_{\theta,t}$ for all $t = 0, \Delta t, \dots, t_f - \Delta t$ to fit (86) to the collected data.

For this example, as we mentioned in Remark 6, we are extending the dimensions of the goal region to all of \mathbf{p} instead of just \mathbf{w} , so $\bar{\mathcal{O}} \subset P$ and $\mathcal{O}_i = \bar{\mathcal{O}}_i \times K$ for all $i = 1, \dots, n_{\mathcal{O}}$. This is such that we can enforce the θ of the car at t_f so the parking is “parallel”. The extension of the goal dimension does not change the other parts of PARC's formulation.

Now we design the parameters in (86). Unlike our other system models, due to the lack of controllability during drifting, the behavior of the realized drift parking trajectories are “open-loop” in that they are uniquely and entirely determined given \mathbf{z}_0 and \mathbf{k} without needing to provide the planning model, as illustrated in Section H.2. As such, we fit a planning model to the data collected in open-loop simulations and use PARC to compute the BRAS of the initial states.

We first collect data by sampling from the pairs $(\mathbf{z}_{0,i}, \mathbf{k}_i) \in Z_{\text{data}} \times K_{\text{data}} \subset Z \times K$ for $i = 1, \dots, n_{\text{data}}$. For the i^{th} data, we denote the realized trajectories $\mathbf{z}_i(t; \mathbf{z}_{0,i}, \mathbf{k}_i) = [p_{x,i}(t), p_{y,i}(t), \theta_i(t), \dots]^\top$ and the sampled trajectory parameters $\mathbf{k}_i = [v_i, \beta_i]^\top$. Then, we can fit the parameters in (86) by

solving the least squares problems:

$$\min_{c_{vx,t}, c_{\beta x,t}, d_{x,t}} \left\| \begin{bmatrix} v_1 & \beta_1 & 1 \\ \vdots & \vdots & \vdots \\ v_{n_{\text{data}}} & \beta_{n_{\text{data}}} & 1 \end{bmatrix} \begin{bmatrix} c_{vx,t} \\ c_{\beta x,t} \\ d_{x,t} \end{bmatrix} - \begin{bmatrix} p_{x1}(t + \Delta t) - p_{x1}(t) \\ \vdots \\ p_{xn_{\text{data}}}(t + \Delta t) - p_{xn_{\text{data}}}(t) \end{bmatrix} \right\|_2^2, \quad (87a)$$

$$\min_{c_{vy,t}, c_{\beta y,t}, d_{y,t}} \left\| \begin{bmatrix} v_1 & \beta_1 & 1 \\ \vdots & \vdots & \vdots \\ v_{n_{\text{data}}} & \beta_{n_{\text{data}}} & 1 \end{bmatrix} \begin{bmatrix} c_{vy,t} \\ c_{\beta y,t} \\ d_{y,t} \end{bmatrix} - \begin{bmatrix} p_{y1}(t + \Delta t) - p_{y1}(t) \\ \vdots \\ p_{yn_{\text{data}}}(t + \Delta t) - p_{yn_{\text{data}}}(t) \end{bmatrix} \right\|_2^2, \quad (87b)$$

$$\min_{c_{v\theta,t}, c_{\beta\theta,t}, d_{\theta,t}} \left\| \begin{bmatrix} v_1 & \beta_1 & 1 \\ \vdots & \vdots & \vdots \\ v_{n_{\text{data}}} & \beta_{n_{\text{data}}} & 1 \end{bmatrix} \begin{bmatrix} c_{v\theta,t} \\ c_{\beta\theta,t} \\ d_{\theta,t} \end{bmatrix} - \begin{bmatrix} \theta_1(t + \Delta t) - \theta_1(t) \\ \vdots \\ \theta_{n_{\text{data}}}(t + \Delta t) - \theta_{n_{\text{data}}}(t) \end{bmatrix} \right\|_2^2, \quad (87c)$$

repeated for each $t = 0, \Delta t, \dots, t_f - \Delta t$. (87) can be solved by any least squares solver. Once (87) is computed, (86) is now a fully defined time-variant affine function that can be used in the PARC framework.

Note that, since (86) is generated only from data with initial conditions in $Z_{\text{data}} \times K_{\text{data}}$, the BRAS is also only valid from within that region. Specifically, when sampling for tracking error à la Section IV-D, one should have $\tilde{Z} \times \tilde{K} \subset Z_{\text{data}} \times K_{\text{data}}$.

For the planning model, we set the timestep $\Delta t = 0.1$ seconds and final time $t_f = 7.8$ seconds.

4) *Environment Details:* In our environment, we define the tracking model state and input bounds to be:

$$\mathbf{z}_{\text{bound}} = \begin{bmatrix} -5, & 40 \\ -20, & 5 \\ -1.5\pi, & 0.5\pi \\ -2, & 1 \\ -0.5, & 20 \\ -\pi, & \pi \end{bmatrix} \quad \mathbf{u}_{\text{bound}} = \begin{bmatrix} 0, & 7684 \\ -0.6632, & 0.6632 \\ -5163, & 5163 \end{bmatrix} \quad (88)$$

We use the geometry specs of the 1981 DeLorean ($l = 4.267, w = 1.988$ m) [39], [40] to represent the car agent as a 2D rectangular H-Polytope \bar{B} . The obstacles $\bar{\mathcal{O}}_{\text{body}_1}, \bar{\mathcal{O}}_{\text{body}_2}$ are two parked car obstacles centered at $[24, -16, -\pi]^\top$ and $[37, -16, -\pi]^\top$ each with the same geometry as \bar{B} .

Next, to ensure that the agent doesn't collide with the obstacles, we create a circular over approximation of \bar{B} as B with a radius of $r = \sqrt{l^2 + w^2}/2$. We then dilate the obstacle into:

$$\begin{aligned} \bar{\mathcal{O}}_1 &= \bar{\mathcal{O}}_{\text{body}_1} \oplus B \\ \bar{\mathcal{O}}_2 &= \bar{\mathcal{O}}_{\text{body}_2} \oplus B \end{aligned}$$

so that as long as the geometrical center of the car agent \mathbf{w} does not enter $\bar{\mathcal{O}}_1$ and $\bar{\mathcal{O}}_2$ as formulated in Problem 4, the trajectory is safe. Note that in this demo, the geometric center and the center of mass coincide.

In this demo, our desired state for the car includes position and orientation states. Therefore we expand the goal set dimension from the previously used workspace dimension \mathbb{R}^{n_w} to the planning state dimension \mathbb{R}^{n_p} by including a range of θ as a goal state. So, we slightly modify Problem 4's goal reaching condition to

$$\text{proj}_{1:n_p}(\mathbf{z}(t; \mathbf{z}_0, \mathbf{k})) \in \bar{P}_G$$

We place the center of the goal in between $\bar{\mathcal{O}}_1$ and $\bar{\mathcal{O}}_2$ at

$$\mathbf{p}_{\text{goal}} = [30.5 \quad -16 \quad -\pi]^\top$$

The goal set \bar{P}_G is then defined as a 3D cuboid H-Polytope centered at \mathbf{p}_{goal} with its length in $[p_x, p_y, \theta]$ as $[3.7, 1.6, \pi/3]$.

Using the drift parking test environment, we collect 10,000 expert trajectories generated by feeding samples of $\mathbf{k} \in K = [9, 11] \times [0.6109, 0.7854]$ into the drift parking controller described above. The initial condition of all trajectories \mathbf{z}_0 is all zeros except for the velocity state $v_0 = 0.01$, as the tracking model experiences numerical instability at low velocities and sideslip angles. The entire simulation process lasts for 2 hours. With the expert trajectories ready, we create the time-variant affine planning model using the formulation above.

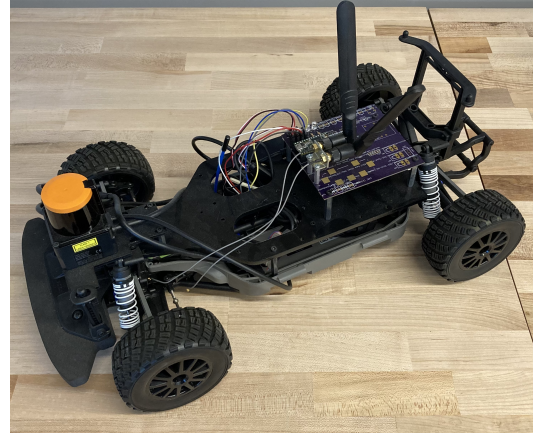


Fig. 12: We are preparing an F1:10 class robotic vehicle to implement and deploy our safe drifting maneuvers. We aim to have a working demo by May 2024.